environments

MDPI

Article

Sustainable Heavy Metal Removal from Model Aqueous Solutions and Industrial Wastewater Using Softwood Sawdust as Eco-Friendly and Cost-Effective Biosorbent

Gamal S. Abdelhaffez [1], Mohamed A. Eltaher [2], Ahmed H. Ibrahim [3] and Amr B. ElDeeb [3,*]

[1] Mining Engineering Department, Faculty of Engineering, King Abdulaziz University, Jeddah 21589, Saudi Arabia; gshassan@kau.edu.sa
[2] Mechanical Engineering Department, Faculty of Engineering, King Abdulaziz University, Jeddah 21589, Saudi Arabia; meltaher@kau.edu.sa
[3] Mining and Petroleum Department, Faculty of Engineering, Al-Azhar University, Nasr City, Cairo 11884, Egypt; ahmedkriaz@azhar.edu.eg
* Correspondence: dr.basuony2016@azhar.edu.eg; Tel.: +20100451972

Abstract

With increasing global concerns about industrial wastewater treatment and the need for sustainable practices, this study explores the potential of softwood sawdust as an eco-friendly, cost-effective adsorbent for removing heavy metal ions, specifically zinc (Zn^{2+}) and lead (Pb^{2+}), from synthetic model solutions. Factors affecting adsorption include adsorbent particle size, pH, adsorbent dosage, and contact time. A remarkable removal efficiency of 98.2% for Zn^{2+} and 98.1% for Pb^{2+} under optimal adsorption conditions of −106 µm average particle size at 8 pH and 0.3 g of adsorbent dosage using 50 (mg/L) initial concentrations for 60 min at ambient temperature. Characterization of the adsorbent used by XRD, FTIR, SEM, and BET analysis confirmed the structural integrity and surface properties of wood sawdust. It is clear that there is a gradual decline in adsorption capacity over multiple reuse cycles due to the depletion of active functional groups. The results confirm wood sawdust's effectiveness as a locally available, low-cost, and biodegradable option for treating wastewater, eliminating metal ions, supporting environmental conservation, and aligning with sustainability goals.

Keywords: wood sawdust; synthetic model solutions; wastewater treatment; sustainability; heavy metal ions; adsorption; mechanism

Check for updates

Academic Editors: Junidah Lamaming and Rafeah Wahi

Received: 17 May 2026
Revised: 26 June 2026
Accepted: 29 June 2026
Published: 7 July 2026

Copyright: © 2026 by the authors. Licensee MDPI, Basel, Switzerland. This article is an open access article distributed under the terms and conditions of the Creative Commons Attribution (CC BY) license.

1. Introduction

Egypt, a semi-arid country, faces water scarcity. The disparity between water availability and demand is widening rapidly amid rapid population growth. Egyptian Vision 2030 aims for sustainable socio-economic growth by expanding industrial and agricultural initiatives. Achieving these initiatives depends on increasing water resource availability and effectively managing industrial waste to reduce environmental impacts [1]. The capacity to augment supplies from the River Nile diminished due to Ethiopia's El-Nahda Dam. Consequently, a viable option to address this gap is the reclamation and treatment of wastewater from various sources [2,3]. Statistical examinations of 37 Egyptian companies suggest that 50% release 1.3 billion cubic meters (BCM) of effluent into the public sewage system annually. This contravenes environmental legislation in Egypt, with only a small portion being treated [4]. Hazardous substances in industrial wastewater damage sewage

infrastructure. This results in higher treatment costs and greater environmental risks associated with sludge disposal [5]. Industrial wastewater is one of the biggest worldwide environmental challenges. The most toxic elements are lead (Pb), cadmium (Cd), chromium (Cr), and nickel (Ni) [6]. While these metals are essential in trace amounts, high levels harm the liver, central nervous system, lungs, kidneys. Removing heavy metal ions from industrial wastewater before discharge is therefore an urgent priority [7]. Heavy metal ion removal from wastewater can be achieved using several methods: adsorption, carbon adsorption, coagulation, membrane filtration, and chemical precipitation [8–13]. Adsorption stands out for being cheap, effective, selective, and chemically insensitive, making it a straightforward and realistic option. Thus, there is a pressing need to develop an adsorbent that is both efficient in removing harmful metal ions from wastewater and is economical and readily available [14].

Economic expansion and industrialization are driving the rise in global industrial waste. Recent worldwide evaluations show that wastewater production exceeds 380 billion m^3 per year, with projections of increases of around 24% by 2030 and 51% by 2050. Almost 80% of global wastewater is released into the environment without sufficient treatment. Industrial sectors contribute significantly by discharging heavy metals, dyes, petroleum hydrocarbons, medicines, and other harmful chemicals into aquatic habitats. As a result, interest is growing in the academic and industry sectors in sustainable wastewater treatment and resource recovery. Water pollution has become a major environmental issue that requires ongoing attention and creative cleanup strategies [15–17].

Numerous strategies have been devised to remediate organic pollutants generated from various activities, including electrochemical methods, photocatalysis, and advanced oxidation processes [18]. In addition to the aforementioned destructive methods, organic contaminants may also be removed using coagulation and coagulation combined with filtration [19]. Inorganic water contaminants often include metal ions and non-metal or metalloid anions. Metals and metalloids, including copper (Cu), cobalt (Co), selenium (Se), iron (Fe), manganese (Mn), vanadium (V), strontium (Sr), and zinc (Zn), are tolerated by living creatures at minimal concentrations; nevertheless, they become poisonous when their levels exceed acceptable thresholds [20].

Recycling solid industrial waste into eco-friendly products is a key priority for sustainable growth, but this goal is hindered by the presence of highly toxic metals. These metals not only threaten environmental quality but also pose health risks to organisms, prompting governments to set strict standards for waterborne metal concentrations. For example, the US EPA mandates drinking water limits for hazardous metals: 1.3 mg/L for Cu, 0.015 mg/L for Pb, 0.01 mg/L for As, 0.005 mg/L for Cd, and 0.1 mg/L for Cr [21].

After primary and secondary treatment, adsorption is used. Primary treatment physically eliminates solid and floating particulates, whereas subsequent treatment biologically destroys most biodegradable organic debris. The treated wastewater may include heavy metals, refractory organic compounds, colors, and trace pollutants [22,23]. Adsorption polishes these pollutants to discharge or reuse requirements. This work proposes wood sawdust as a cost-effective adsorbent for tertiary treatment of industrial wastewater containing Zn^{2+} and Pb^{2+} ions, improving treatment efficiency and sustainability [24–27]. The use of biomass-derived adsorbents has emerged as an eco-friendly method for extracting heavy metals from industrial effluents. Recent comparative studies indicate that steam-activated spruce sawdust adsorbents achieve an optimum Fe^{2+} ion adsorption capacity of 329 mg/g, while steam-activated waste from the wine industry exhibits a maximum Pb^{2+} ion adsorption capacity of 399 $mg \cdot g^{-1}$ [28].

KOH-impregnated Hevea brasiliensis sawdust-derived activated carbon (CMHBS) was examined to remove Pb, Cd, and Ni from synthetic wastewater. The adsorbent's

large specific surface area (511.51 m^2 g^{-1}) and microporosity enabled effective heavy-metal adsorption. Multi-metal systems exhibited an antagonistic effect, with adsorption preference in the order Pb^{2+} > Cd^{2+} > Ni^{2+}. Adsorption was best represented by the Langmuir model for single-metal systems and the Freundlich model for multi-metals, whereas kinetics followed the pseudo-second-order model. Adsorption was spontaneous and exothermic, according to thermodynamics. After four rounds of regeneration with 0.2 M HCl, the adsorbent maintained removal efficiency. The research showed that KOH-modified H. brasiliensis sawdust may remove heavy metals from wastewater cheaply and sustainably [29].

Pine sawdust-derived adsorbents removed heavy metals and phenol from simulated industrial wastewater. Steam-activated sawdust (SAS) removed Pb and Zn as well as commercial activated carbon due to its physicochemical features and specific surface area. The Freundlich isotherm best explained metal ion equilibrium data, whereas the Langmuir model described phenol adsorption. Kinetic investigations showed Cr adsorption followed the pseudo-second-order model, supporting chemisorption. SAS might be an inexpensive ($52 per kg) and ecologically friendly industrial wastewater treatment adsorbent, since its manufacturing cost was far lower than commercial activated carbon ($80–300 per kg) [30].

Hevea brasiliensis wood sawdust (HBS) was tested as a low-cost biosorbent for Cd(II), Pb(II), and Ni(II) removal from single- and multi-metal wastewater systems [31]. The order of adsorption performance was Pb(II) > Cd(II) > Ni(II), with best removal at pH 5.0, 7 $g{\cdot}L^{-1}$ adsorbent dose, and 90 min contact time. Adsorption kinetics fitted the pseudo-second-order model, but equilibrium data fit the Langmuir isotherm. Competitive adsorption in binary and ternary systems lowered metal absorption more than single-metal systems. BET, FTIR, SEM, and EDS showed that electrostatic attraction and surface complexation dominated adsorption. Real wastewater was treated by the adsorbent at a low cost of $0.021 per liter of mixed-metal effluent, demonstrating its economic and environmental promise for wastewater remediation.

Treated and untreated Cedrus deodara sawdust were tested as a low-cost biosorbent for Cd(II) ion removal and pre-concentration from aqueous solutions [32]. Adsorption was fast, removing 97% Cd(II) in 8 min, and pH-dependent, with optimal absorption between pH 4 and 8. Metal-binding carboxylic and amine functional groups were found by potentiometric titration. The Langmuir and Dubinin–Radushkevich (D–R) isotherm models well represented the equilibrium data, and kinetic and thermodynamic investigations validated the strength of the adsorption process. Sawdust was an effective, low-cost material for cadmium removal, as evidenced by quantitative recovery of Cd(II) via HCl desorption.

Walnut and cherry wood-processing wastes and hydropyrolysis-derived biochars were tested as sustainable Mn(II) adsorbents in aqueous solutions [33]. The biochars had somewhat greater adsorption capabilities (2.4–2.5 $mg{\cdot}g^{-1}$) than raw wood shavings (2.1–2.2 $mg{\cdot}g^{-1}$). Adsorption kinetics followed the pseudo-second-order model, showing chemisorption on heterogeneous surfaces, whereas equilibrium data were best explained by the Freundlich model for cherry-based adsorbents and the RALF isotherm for walnut-based materials. The results showed that wood-industry wastes and biochars are effective, low-cost, and ecologically sustainable manganese adsorbents, promoting circular economy and wastewater treatment.

In a study [34], unmodified Norway Spruce Wood Residue (NSWR) was tested for its ability to remove Pb, Cd, Zn, and Cu from a quaternary aqueous system. Batch adsorption trials showed 60% metal absorption in 20 min and best performance at slightly acidic conditions (pH 5–6). Maximum Langmuir adsorption capabilities were Pb^{2+} (10.3 $mg{\cdot}g^{-1}$) followed by Cu^{2+} (7.9 $mg{\cdot}g^{-1}$), Cd^{2+} (6.3 $mg{\cdot}g^{-1}$), and Zn^{2+} (6.0 $mg{\cdot}g^{-1}$), with Pb^{2+} achieving up to 99% removal efficiency The Langmuir isotherm (R^2 = 0.99) accurately

represented equilibrium data, showing effective mono-layer adsorption. Adsorption occurred via surface functional group interactions and cation-exchange processes, according to FTIR and EDS. NSWR treated multi-metal-contaminated wastewater effectively, cheaply, and sustainably, according to the research.

Raw Eucalyptus globulus sawdust was tested as a low-cost biosorbent for Pb(II) removal from aqueous solutions [35]. A heterogeneous porous structure including functional units such as hydroxyl, carboxyl, amine, and hydrocarbon moieties contributed to metal binding, as shown by SEM and FTIR. Successful batch adsorption tests at pH 6 achieved 96% Pb(II) removal efficiency and 4.80 $mg \cdot g^{-1}$ adsorption capacity. Both Langmuir and Freundlich isotherms accurately captured equilibrium data, but the pseudo-second-order model better explained adsorption kinetics. Ion exchange between Pb(II) ions and biomass functional groups was the main adsorption process. The research found that eucalyptus sawdust adsorbs lead-contaminated wastewater economically.

According to [36], ozone-modified acacia sawdust biochar efficiently eliminated nitrogen from pig effluent, with an adsorption capacity of 32.38 $mg \cdot g^{-1}$. The adsorption process conformed to pseudo-second-order, Elovich, and Freundlich models, signifying heterogeneous chemisorption. The research further established the economic viability and reusability of biochar, positioning it as a viable low-cost adsorbent for the treatment of agricultural wastewater.

The petroleum industry's profit margins and productivity are often hindered by issues related to emulsified water [37–40]. Demulsification, the process of separating saline water from crude oil into two distinct phases, is necessary prior to the transportation or refining of crude oil to avoid economic losses and operational issues [41]. Demulsification is typically achieved using a suitable demulsifier [42]. Reported techniques for crude oil demulsification fall into three main categories: chemical, physical (including mechanical, thermal, microwave, electrical, ultrasonic, and membrane), and biological [43]. Chemical demulsification is the most widely used method, relying on the addition of demulsifier to crude oil emulsions [44]. These chemical additives primarily destabilize the emulsifying agents [45]. The generated oil must meet the pipeline's and the corporation's requirements; hence, these features are crucial. It is standard practice for crude oil processing facilities to limit the amount of salt and basic sediment and water in the finished product to no more than 10 pounds per thousand barrels of crude oil, or 0.2% [46]. This standard, however, differs from one firm to the next and from one pipeline to another. Finding a reliable method for demulsifying crude oil emulsions is a key research focus in the crude oil processing industry [47].

In this context, the industrial wastewater extracted by an appropriate demulsifier technique is discharged into coastal zones or well drains so, it must be treated to remove refractory organic polymers, which are very harmful to aquatic organisms, posing serious health hazards to all inhabitants and endangering the biological ecosystem of the region prior to being discharged into the environment [48]. While several governments have established wastewater standards for agricultural irrigation, the US EPA and the WHO have proposed and revised water quality criteria or standards to ensure the safe reuse of wastewater [21,49]. The Egyptian government has enacted a number of environmental laws and regulations. Egyptian Presidential Decree No. 631/1982 created the Egyptian Environmental Affairs Agency [50]. Key contaminants in trade effluents include organic materials, nutrients such as nitrogen and phosphorus, petroleum products, hydrocarbons, and metals like lead, zinc, and mercury. These pollutants harm marine life, ecosystems, and human health.

Therefore, this research examines the adsorption capacity of natural softwood sawdust to remove Zn and Pb metal ions from synthetic model solutions. The study aims

to: (1) optimize operational parameters (pH, contact time, adsorbent dose, metal concentration) through statistical methods; (2) elucidate adsorption mechanisms utilizing Langmuir/Freundlich isotherms and kinetic models; (3) assess adsorbent reusability over multiple adsorption–desorption cycles; and (4) implement this adsorbent for reducing heavy metal ion concentrations in an industrial wastewater sample sourced from the Egyptian General Petroleum Corporation (EGPC).

2. Materials and Methods

2.1. Materials

The experimental work used softwood sawdust collected from a wood chipper plant. Chemically pure reagents (NaOH, HCl) were purchased from Sigma-Aldrich. In this work, analytical-grade chemical reagents $ZnSO_4 \cdot 7H_2O$ and $Pb(NO_3)_2$ were used to prepare standard synthetic model solutions of Zn^{2+} and Pb^{2+} by dissolving these salts in double-distilled water. These solutions were treated individually (single-component) with wood sawdust to assess adsorption efficiency under various conditions. The wastewater sample used in this investigation was collected from EGPC-owned land prior to disposal. A cotton membrane was used to filter the wastewater sample, removing suspended debris and oils.

2.2. Methods

2.2.1. Preparation of Softwood Sawdust (WS) Materials

The softwood sawdust sample was ground and mixed thoroughly. Then, the ground sample was dried in a drying oven at 110 °C for 6 h then the dried sample has been kept in a desiccator before application. After, grinding, mixing, coning, and quartering technique has been done to obtain a representative sample of about 300 g for different physiochemical analysis. A nest of sieves, namely, 1000 µm, 500 µm, 250 µm and 106 µm sieves was used to fractionate the sample.

2.2.2. Materials Characterizations

The characterization techniques employed in this study are as follows: X-ray diffraction (XRD) (Analytical X-Ray Diffraction equipment model X" Pert PRO with Monochromator, Cu-Kα radiation (λ = 1.542 A) at 40 mA, 50 KV and scanning speed 0.02/s). Carbon–Sulfur (CHNS) (Perkin Elmer: model Series II CHNS/O 2400) analyzer. Inductively coupled plasma atomic mass spectrometry (ICP-MS, Perkin Elmer ELAN model 9000 USA) was used to precisely ascertain the concentration of metal ions in synthetic model solutions and industrial wastewater samples before to and during the adsorption procedure. Microstructural and elemental analyses of the sawdust were performed using a Tescan TS 5130MM scanning electron microscope (SEM) equipped with an energy dispersive X-ray (EDX) detector (fabricated by Oxford Instruments with an active crystal area of 50 mm^2), alongside a microanalysis system and a YAG crystal as a back-scattered electron (BSE) detector. Fourier Transform Infrared (FT-IR) spectroscopy, model Bruker ALPHA, was used to analyze the sawdust sample and examine its chemical characteristics. The Brunauer–Emmett–Teller (BET) technique for multilayer adsorption was used to ascertain the specific surface area of the sawdust. The Barret Joyner and Halenda (BJH) techniques were used to ascertain the pore volume and average pore diameter. The sample was degassed for 12 h at 300 °C before the test, and the nitrogen adsorption-desorption measurement was conducted at liquid nitrogen temperature (77 K). The mean particle size of softwood sawdust was determined using a particle size analyzer (Malvern Instruments Hydro 2000S Master Size, Malvern, UK).

2.2.3. Point of Zero Charge (pH_{ZPC})

The procedure entails dissolving 10 mg of the material in 20 mL of a 0.1 M NaCl solution. The original pH value (pH_i) of the NaCl solution was adjusted from 1 to 12 by adding 0.1 M HCl and 0.1 M NH_4OH. The suspension attained equilibrium at 25 ∘C after 24 h of stirring. The solution was then filtered, and the final pH value (pH_f) was assessed [51]. The pH_{ZPC} was derived using the graph of pHi and pH_f data. The same technique was performed in a 0.01 M NaCl solution. When the pH equals the pH_{ZPC}, the surface is neutral. If the pH_{ZPC} exceeds the solution's pH, the adsorbent surface has a positive charge. When the pH exceeds the pH_{ZPC}, the surface acquires a negative charge. The pH_{ZPC} of the samples was determined using the batch equilibration approach.

2.2.4. Adsorption Experiments

The adsorption efficiency of sawdust for Zn^{2+} and Pb^{2+} ions from prepared synthetic model solutions samples was evaluated in batch adsorption tests. The main goal of the research was to determine how various variables affect adsorption efficiency. These variables include pH (a measure of acidity), contact duration (time during which adsorbent and solution interact), adsorbent dose (amount added), and initial metal ion concentration (amount of metal ions in solution at the start). The tests were conducted in 200 mL conical flasks. 100 mL of Zn ion solutions and 150 mL of Pb ion solutions were combined with a sorbent dosage of 0.3 g at room temperature. The solutions had different concentrations of 50 ppm. With solutions of 0.1 M HCl and 0.1 M NaOH, the pH was changed. Subsequently, the suspension was agitated on a rotary shaker at 200 rpm for 10–120 min, with a pH range of 2–11, to achieve a uniform, equilibrium concentration of metal ions. Filtration was used to remove the adsorbent from the metal-ion solutions after the specified contact time had elapsed. The solutions were then analyzed by Inductively Coupled Plasma Atomic Mass Spectrometry (ICP-MS) to determine the amounts of heavy metal ions. We tested wood sawdust under these ideal adsorption conditions to determine how well it removed Zn and Pb ions.

The equilibrium metal ion adsorption per mass of the adsorbent is reported here. Equations (1) and (2) calculated the removal efficiency (%) and equilibrium loading (q_e, $mg{\cdot}g^{-1}$) of a specific metal ion.

$$R.E.(\%) = \left[\frac{(C_0 - C_t)}{C_0}\right] \times 100 \quad (1)$$

$$q_e\left(mg{\cdot}g^{-1}\right) = \frac{(C_0 - C_t) \times V}{m_s} \quad (2)$$

In this context, *R.E.* (%) is the removal efficiency of a particular metal ion in percentage form, q_e is the absorption capacity in ($mg{\cdot}g^{-1}$), C_0 is the starting concentration of metal ions in the solution in ($mg{\cdot}L^{-1}$), C_t is the equilibrium concentration at a given time in ($mg{\cdot}L^{-1}$), V is the volume of the solution (L), and m_s is the mass of the adsorbent (g).

2.2.5. Desorption

Desorption tests were conducted to evaluate the practical usefulness of the adsorbent. In the desorption experiment, 0.3 g of metal-loaded sorbent was agitated in 100 mL of 0.1 M HCl at 25 °C [52]. Following 60 min of agitation at 400 rpm, the metal content in the solution was assessed. The adsorption and desorption processes were repeated 4 times to obtain the optimal eluent.

Conversely, the desorption process may be assessed in terms of the adsorbent's reusability, characterized by its regeneration capacity or efficiency. Regeneration capacity

(*R.C.*) is defined as the difference between the adsorption capacity of an adsorbent material post-desorption cycles and its initial adsorption capacity, as determined by Equation (3).

$$\boldsymbol{R.C.}(\%) = \left[\frac{q_r}{q_0}\right] \times 100 \quad (3)$$

where *qr* is the adsorption capacity of a given adsorbent after a regeneration process, and q_0 is its original adsorption capacity.

All tests were conducted in duplicate, and the mean data were used in the computations. The greatest variance was determined to be ±2%. All model parameters were assessed by linear regression utilizing Origin Pro. 9 software. This research examines frequently used error functions, namely the correlation coefficient (R^2).

3. Result and Discussion

3.1. Composition of the Softwood Sawdust

The specific surface area of solids may be calculated using solid adsorption measurements using BET method. Figure 1 displays the findings of an investigation into the surface properties of wood sawdust using the N_2 adsorption–desorption technique. There is a class H3 hysteresis loop and a type IV isotherm in the sawdust. The structure of sawdust is characteristic of mesoporous and macropore materials, as shown by its strong adsorption at low relative pressures ($P/P_0 < 0.1$). The distribution of particle size for sawdust (PSD) is shown in Figure 2 and Table 1. Based on the PSD, the wood sawdust had median particle sizes of around 10 and 20 µm, meaning that 50% and 90% of the particles, respectively, were within these dimensions. Particle size distribution plays a pivotal role in adsorption processes because more surface area provides more active binding sites, thereby improving the removal of heavy metal ions from the solution of interest [53]. The key information of the surface characteristics of sawdust is provided in the Table 2. Table 2 lists various parameters and properties related to the characterization of the sample. These data provides detailed information about the physical and surface properties of the sample, which can be useful for characterizing materials and understanding their potential applications [54].

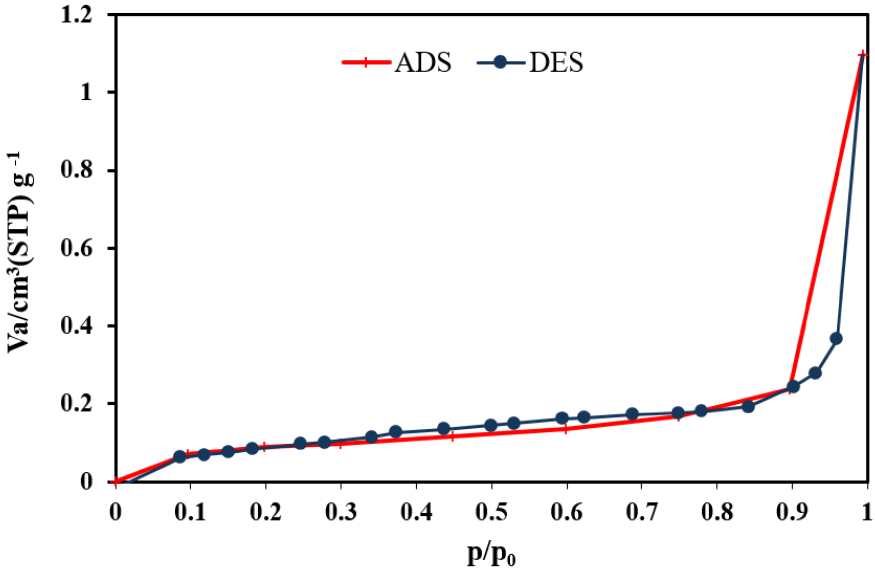


Figure 1. N_2 adsorption—desorption isotherms.

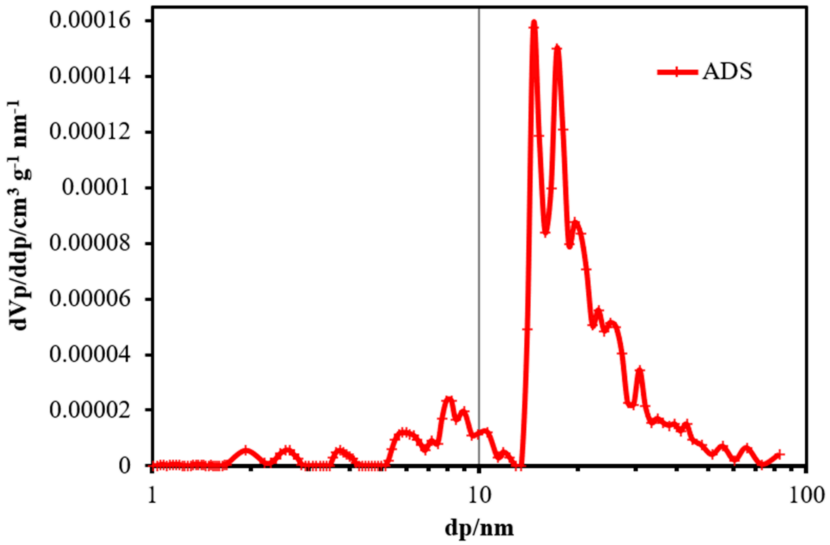


Figure 2. Pore size distribution plot of wood sawdust.

Table 1. The particle size distribution of used sawdust.

No.	Size	Weight (g)	Percentage (%)
1	(+1000)	8	3.16
2	(−1000 + 500)	73	28.85
3	(−500 + 250)	113	44.67
4	(−250 + 106)	50	19.76
5	(−106)	9	3.56
	Total	253	100

Table 2. The surface characteristics of sawdust (BET).

V_m [cm^3 (STP)·g^{-1}]	0.07181
BET [m^2·g^{-1}]	302.55
Total pore volume, [cm^3·g^{-1}]	0.0188
Average pore diameter, [nm]	12.025

Figure 2 displays the pore size distribution of the sample (sawdust). The sharp peak in the plot indicates the presence of a predominant pore size in the sample. The shape and width of the peak provide information about the pore size uniformity and distribution within the material. This type of analysis is commonly used to characterize the porous structure and surface properties of materials, which are important for different applications such as adsorption, catalysis, and filtration [54].

Figure 3 shows the zeta potential, the electrical potential that exists at the shear plane—the boundary between the stationary layer of fluid attached to the particle's surface and the mobile part of the surrounding liquid. This potential difference is an important indicator of the degree of repulsion or attraction between particles in a dispersion.

The point of zero charge (pH_{zpc}) of the wood sawdust was determined using the pH drift technique. Figure 3 shows that the plot of (pH_f–pH_i) against starting pH intersects the zero line at around pH 7.0, indicating no net charge at this pH_{zpc}. Below the pH_{zpc}, the wood sawdust surface is predominantly positively charged due to protonation of surface functional groups; conversely, above the pH_{zpc}, deprotonation yields a negatively charged surface. Consequently, adsorption behavior is significantly affected by solution pH, with increased adsorption of cationic species anticipated at pH levels above the pH_{zpc} due to advantageous electrostatic interactions. In these circumstances, cationic pollutants

are enhanced by electrostatic attraction, whereas anionic species may be obstructed by electrostatic repulsion [55].

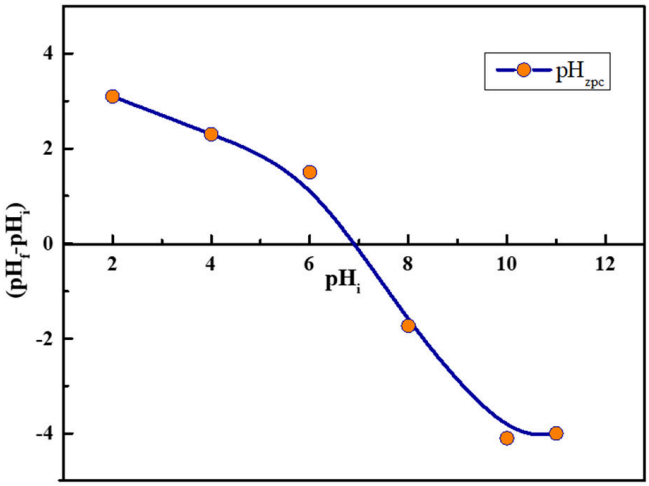


Figure 3. Determination of (pH_{ZPC}) of wood sawdust.

The SEM study indicates that the raw biomass exhibits a coarse, fibrous, and heterogeneous surface morphology characterized by numerous grooves, fissures, and inter-fiber spaces (Figure 4). These attributes facilitate chemical activation and are anticipated to augment the development of adsorption sites, elevate surface area, and promote the diffusion of pollutants into the adsorbent matrix. Consequently, biomass has considerable promise as a precursor for the fabrication of high-performance adsorbents aimed at environmental remediation, namely, for the extraction of heavy metals and nutrient contaminants from industrial wastewater [25].

The spectrum shows the different X-ray peaks corresponding to the chemical elements present in the sample. The peak for Oxygen (O) is located around the 0.5 keV mark on the x-axis and reaches approximately 2000 counts on the y-axis, indicating its prominent presence in the sample. The Carbon (C) peak appears near the 0.2 keV region, with a peak intensity of roughly 4500 counts, making it the highest peak in the spectrum. Additionally, the analysis reveals trace amounts of other elements, including aluminum (Al) at 1.5 keV, magnesium (Mg) at 1.2 keV, silicon (Si) at 1.8 keV, sulfur (S) at 2.3 keV, and sodium (Na) at 1 keV, as shown in Figure 5. Table 3 presents the composition percentages for the elements found in the sample: Carbon (C) ranges from 43.1% to 55.7%, while Oxygen (O) varies from 54.3% to 55.7%. Sodium (Na) is present at 0.3% to 0.4%, and Magnesium (Mg) is found at 0.2% to 0.4%. Aluminum (Al) ranges from 0.5% to 0.6%, Silicon (Si) is between 0.9% and 1.0%, and Sulfur (S) shows a concentration of 0.1% to 0.6%. Additionally, Calcium (Ca) varies from 0.3% to 0.7%, and Iron (Fe) is present at 0.4% to 1.0%. Titanium (Ti) and Potassium (K) were not detected in the sample.

The Fourier Transform Infrared Spectroscopy of sawdust (FTIR) analysis method uses infrared light to scan sawdust sample and observe chemical properties. Figure 6 shows a plot that is commonly used in infrared (IR) spectroscopy to analyze the absorption or transmittance characteristics of a sample across different infrared wavelengths.

The x-axis covers a wide range of wavenumbers, from around 4000 cm^{-1} to 500 cm^{-1}, which represents the mid-infrared region of the electromagnetic spectrum. The transmittance values are plotted on the y-axis, ranging from around 65% to 125%. The spectrum exhibits multiple absorption bands or dips in the transmittance, which indicate the presence of specific functional groups or molecular vibrations in the sample. The most prominent absorption band appears around 3350 cm^{-1}, which is typically associated with O-H stretch-

ing vibrations, indicating the presence of hydroxyl groups or water in the sample. The peak observed at 2906 cm^{-1} indicates the stretching of the CH_3 group. Additionally, a significant absorption band is noted around 1900 cm^{-1}, which may be associated with C=O stretching vibrations [34]. The peak at 1253 cm^{-1} provides insight into the C-O stretching vibration of hemicellulose. Furthermore, the presence of halogen groups (C-O-C) is confirmed by peaks at 1022 cm^{-1} and 514 cm^{-1} [56].

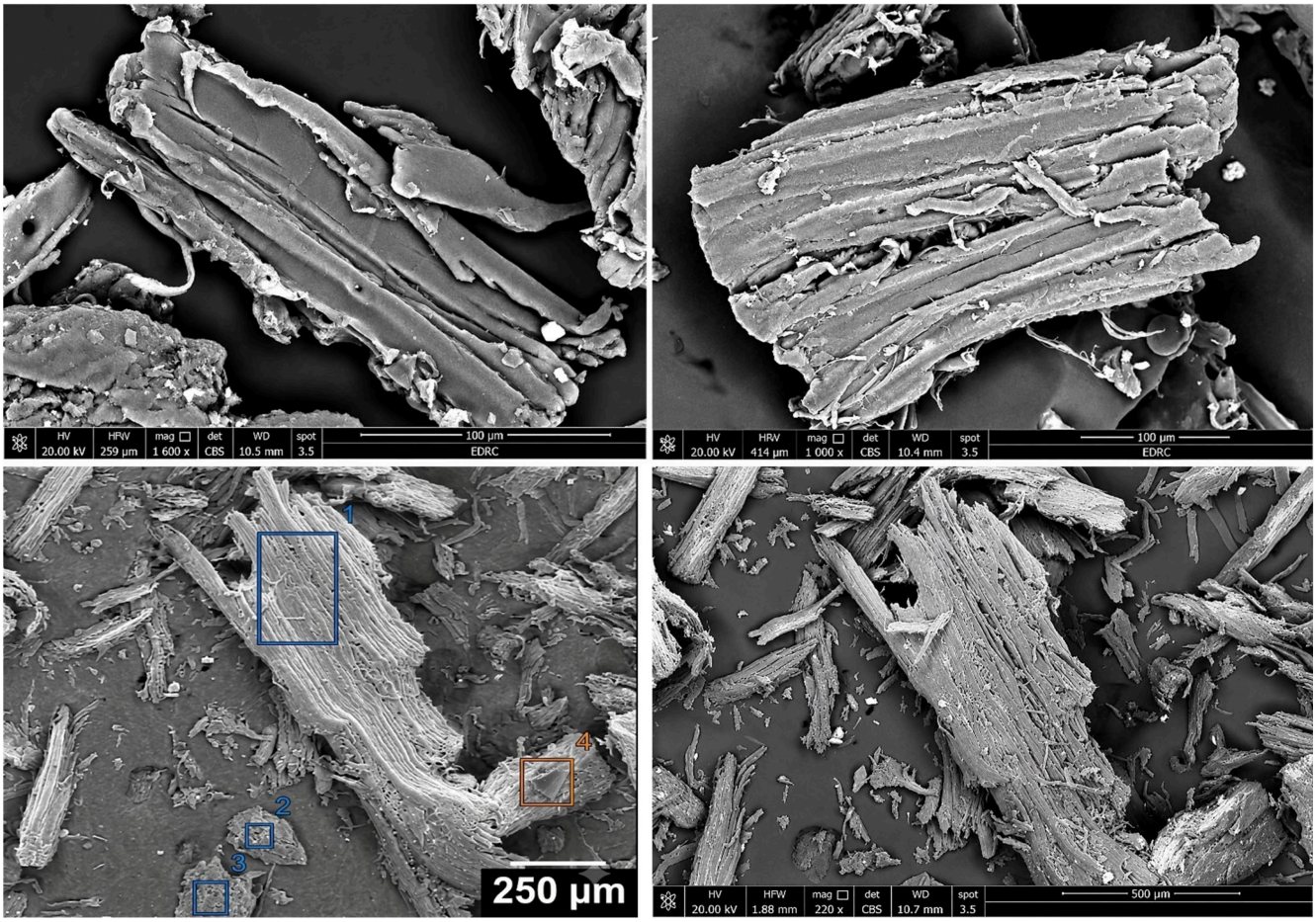


Figure 4. SEM image at various locations on the surface structure of wood sawdust sample.

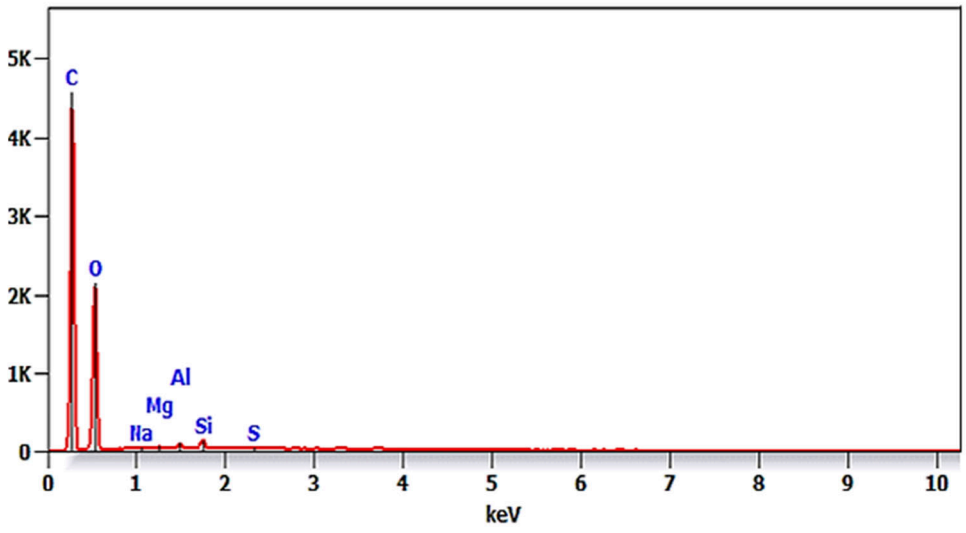


Figure 5. EDS elemental analysis on the whole surface structure of wood sawdust.

Table 3. Elemental composition at various points on the wood sawdust surface with stander deviation (S.D).

Locations	C	O	Na	Mg	Al	Si	S	Cl	K	Ti	Fe
location 1	43.1	54.3	0.3	0.4	0.6	1.0	0.3	-	-	-	-
location 2	42.8	53.7	0.3	-	0.4	0.5	0.4	-	-	0.7	1.0
location 3	43.9	55.6	-	-	0.2	0.3	-	-	-	-	-
location 4	40.8	55.7	0.4	0.2	0.5	0.9	0.6	0.1	0.3	-	0.4
S.D.	42.65	54.825	0.25	0.15	0.425	0.675	0.325	0.025	0.075	0.175	0.35

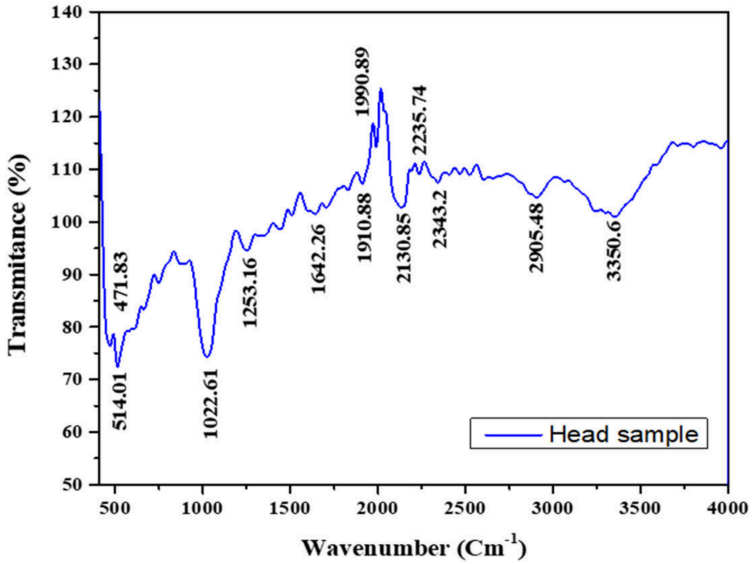


Figure 6. FTIR of wood sawdust sample.

X-ray diffraction analysis (XRD) of the used wood sawdust sample is illustrated in Figure 7. The sharp, well-defined peak around 2-theta = 22.5 degrees is a characteristic peak for the crystalline cellulose structure in the sawdust. The broad, less intense peaks in the 2-theta range of 10–30 degrees also indicate the presence of the amorphous components, such as hemicellulose and lignin, in the sawdust. The overall XRD pattern suggests that the sawdust sample has a partially crystalline structure of heavy metal ions, underscoring the need for more detailed analysis of trace mineral phases [34,57,58].

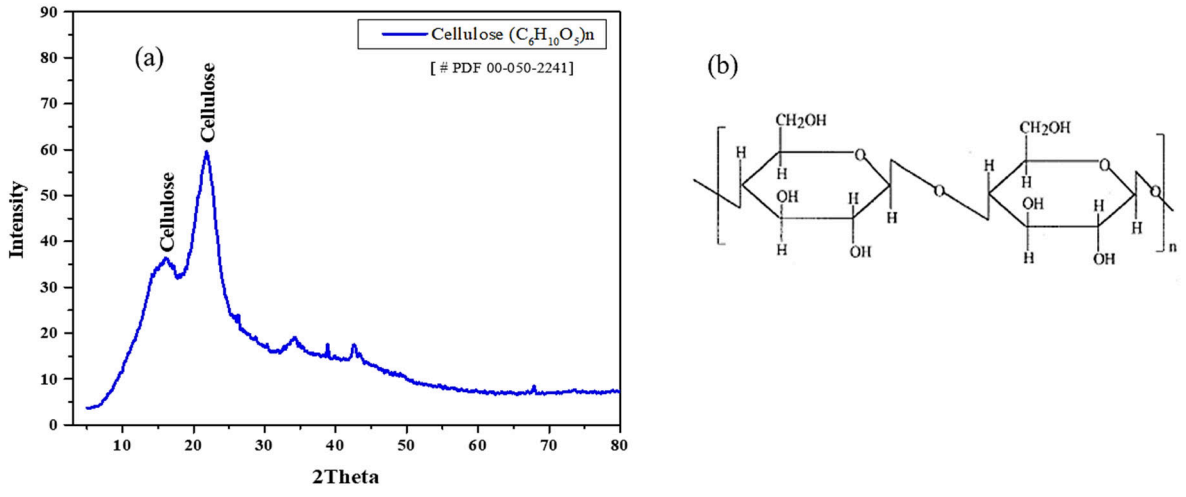


Figure 7. (**a**) XRD Patterns of wood sawdust sample and (**b**) structure of cellulose.

Table 4 presents a detailed analysis of the composition of wood sawdust (WS), highlighting the various components that contribute to its overall makeup. The predominant element in wood sawdust is Carbon (C), which accounts for a significant percentage, reflecting the organic nature of the material. Following closely is Oxygen (O), essential for the biochemical processes that characterize wood.

Table 4. The chemical composition of different types of wood sawdust (WS) and major content.

Sawdust	Elemental Compositions (%)				References
	C	H	O	N	
Pine sawdust	46.41	6.27	47.23	0.06	[59]
Meranti sawdust	42.38	5.27	42.41	0.14	[60]
Chinese fir sawdust	48.95	6.54	53.74	0.11	[61]
Rubber-wood sawdust	44.0	8.04	47.5	0.45	[62]
Sawdust (Canada)	45.2	6.7	48.0	0.1	[63]
Wood sawdust	48.12	5.93	45.49	0.46	Current Study
Major Chemical Constituents of Wood Sawdust in the Present Study (%)	**Content (%)**				
Cellulose (alpha)	40.38				
Hemicellulose	29.51				
Lignin	26.26				
Extractives	3.08				
Ash	0.64				

The chemical composition of the analyzed biomass presented in Table 4 indicates that it is predominantly lignocellulosic, comprising cellulose (40.38%), hemicellulose (29.51%), and lignin (26.26%), with negligible quantities of extractives (3.08%) and ash (0.64%). The significant quantity of structural carbohydrates (cellulose and hemicellulose, totaling 69.89%) suggests a prevalence of hydroxyl (OH^-) groups, which may serve as active sites for metal ion binding via hydrogen bonding, ion exchange, and surface complexation. Lignin has a network structure mostly of methoxy and free hydroxyl groups. Accordingly, these features make the material a suitable precursor for the manufacture of biosorbents and possess the ability to adsorb diverse heavy metal ions [32,64].

3.2. Optimization of Metal Ion Adsorption on Wood Sawdust

3.2.1. Effect of Sawdust Particle Size

The effect of sawdust particle size in the adsorption of heavy metal ions from standard synthetic model solutions has been investigated by using different size fractions +1000 µm, −1000 + 500 µm, −500 + 250 µm, −250 + 106 µm and −106 µm and carried out at fixed operating conditions of 7 pH, 30 min contact time, 0.2 g dosage of adsorbent and at 25 °C. It is clear that as the particle size of sawdust decreases from coarser to finer fractions (from sample 1 to sample 5), while the removal efficiency for both Pb and Zn increases, as presented in Figure 8.

This trend leads to a reduction in the concentrations of these metal ions in synthetic model solutions as the particle size becomes finer. Notably, the finest particle size fraction (−106 µm) exhibits the highest removal efficiencies, achieving 41.6% for Zn and 47.6% for Pb. This pattern suggests that the adsorption capacity of sawdust is inversely related to particle size; smaller particles provide a greater surface area for adsorption, thus enhancing the removal of heavy metal ions from synthetic model solutions. The obtained results indicate that optimizing the particle size distribution of sawdust as an adsorbent could significantly

improve the effectiveness of heavy metal ions removal from contaminated water [65–67]. The particle size of −106 µm demonstrated the greatest efficiency in extracting heavy metals; hence, this size was selected as the optimum particle size and was used for subsequent optimization of the other parameters.

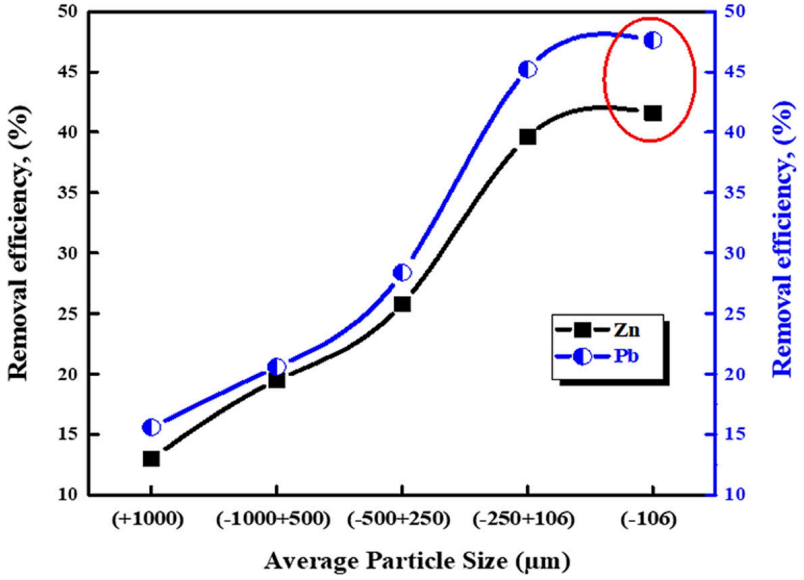


Figure 8. Effects of sawdust particle size on the adsorption efficiency of Zn^{+2} and Pb^{+2} metal ions.

3.2.2. Effect of pH

The surface charges of the adsorbent and the extent to which the adsorbate is ionized and speciated are affected by the pH value of the aqueous solution, which is a major determinant in the adsorption process. Figure 9 shows how the adsorption of Zn^{2+} and Pb^{2+} metal ions are affected by pH levels ranging from 2.0 to 11.0.

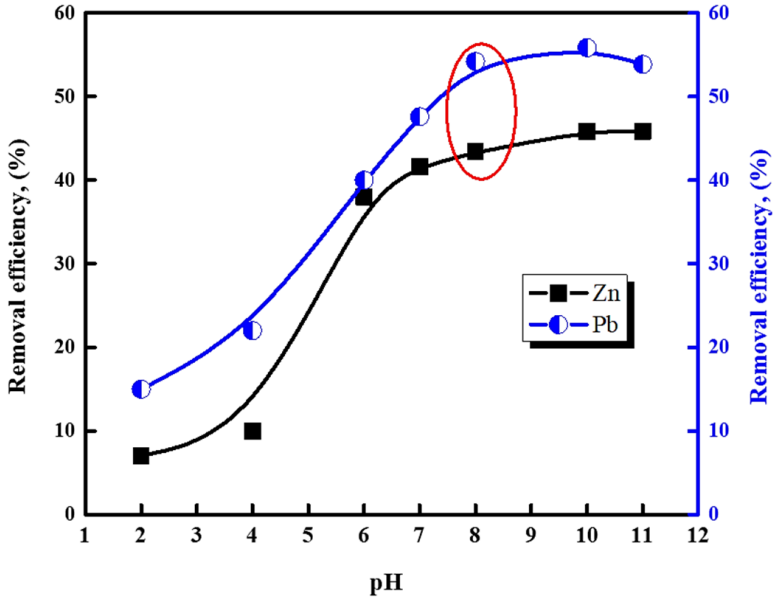


Figure 9. Impact of pH values on the adsorption efficiency of Zn^{+2} and Pb^{+2} ions.

It was shown that the adsorption effectiveness of metal ions increases with increasing pH. Increasing the solution pH from 2 to 8 resulted in 7% and 15% increases in Zn^{2+} and Pb^{2+} removal efficiency, respectively. Based on these findings, a pH of 8 or higher is

recommended for maximum elimination of Zn^{2+} and Pb^{2+} [68]. The process of metal ion exchange with hydrogen ions is described by the following Equations (4)–(9).

$$X - OH + H_3O^+ \rightarrow X - OH_2^+ + H_2O \qquad (X = C, O, \text{ etc. }) \tag{4}$$

$$X\text{–}OH_2^+ + M^{2+} \rightarrow X - O - M \qquad (M = Zn, Pb) \tag{5}$$

$$X - OH + OH^- \rightarrow X - O^- + H_2O \tag{6}$$

$$2(X - O^-) + M^{2+} \rightarrow X - O - M - O - X \tag{7}$$

$$M^{2+} + H_2O \rightarrow M(OH)^+ + H^+ \tag{8}$$

$$X - OH + M(OH)^+ \rightleftarrows XM(OH)_2 \tag{9}$$

There is a correlation between the pH and the zeta potential (ZPC) for a particular sawdust sample, as shown in Figure 3. The surface of sawdust hydrates in a very acidic environment, becoming positively charged from an abundance of hydrogen ions (Equation (4)) and partly replaced by metal ions (M^{2+}) (Equation (5)). Partial destruction of the sawdust structure reduced metal-ion adsorption. The adsorption capacity was further reduced when cationic ions and H^+ ions competed for active sites [6]. On the other hand, pH was observed to affect the adsorbent's adsorption capacity. This is because a rise in pH causes the dissociation of hydroxyl groups on the surface of the adsorbent, leading to an increase in the negative charge (Equation (6)). Equation (7) indicates that electrostatic attraction increases between metal ions and sites on solid surfaces [69]. After adsorption, cationic ions react with OH^- to form hydrated heavy-metal cations, $M(OH)^+$. This process increases the concentration of H^+ ions and raises the pH, as shown in Equation (8). Following this, the hydroxyl group reacts with the hydrated $M(OH)^+$ to produce precipitation chemicals on the adsorbate surface (Equation (9)) [13].

As the pH of standard synthetic model solutions rises from 2 to 11, the removal efficiency for both Pb and Zn improves markedly as illustrated in Figure 9. At the lowest pH value of 2, the Pb and Zn removal efficiencies are quite low, at 7% and 15% respectively. The removal efficiencies for both metals improve drastically as the pH increases, reaching 43.36.6% for Zn and 54.2% for Pb at the highest pH value of 8. These results indicate that the adsorption of Pb and Zn onto the adsorbent material is highly pH dependent. The enhanced removal at higher pH values is likely due to the changes in the surface charge and speciation of the metal ions, which enhances their interaction and adsorption onto the adsorbent [68].

3.2.3. Effect of Adsorbent Dosage

The data shown in Figure 10 illustrates the relationships between adsorbent dose, removal efficiency, and adsorption capacity of heavy metal ions by sawdust. Volumes of 100 mL of zinc metal solution and one hundred milliliters of lead metal solution were mixed with adsorbent dosages ranging from 0.05 $g{\cdot}L^{-1}$ to 0.4 $g{\cdot}L^{-1}$ in order to study the effect of adsorbent dosage. The removal efficiency for both Zn and Pb increases substantially when the adsorbent dose is doubled from 0.05 to 0.4 $g{\cdot}L^{-1}$. Specifically, the Zn removal efficiency rises from 3% at the lowest dosage to 82.86% at the highest dosage. Similarly, the Pb removal efficiency improves from 4% to 91.4% with increasing the adsorbent dosage, as illustrated in Figure 10A. As shown in Figure 10B, the maximum adsorption capacities for Zn^{2+} and Pb^{2+} were determined to be 13.78 and 22.85 $mg{\cdot}g^{-1}$, respectively, at an adsorbent dosage of 0.3 $g{\cdot}L^{-1}$. The findings show that the effectiveness of the sawdust adsorbent in removing Pb and Zn from synthetic model solutions increases with increasing dose. This is most likely because adsorption sites and surface area become more abundant with

increasing adsorbent amounts, enabling the effective absorption of heavy metal ions [69,70]. The maximum removal rates for both Zn and Pb were therefore obtained with a sawdust content of 0.3 g·L^{-1}, which also produced the best removal efficiency for heavy metal ions. The remaining parameters were then optimized using this dose.

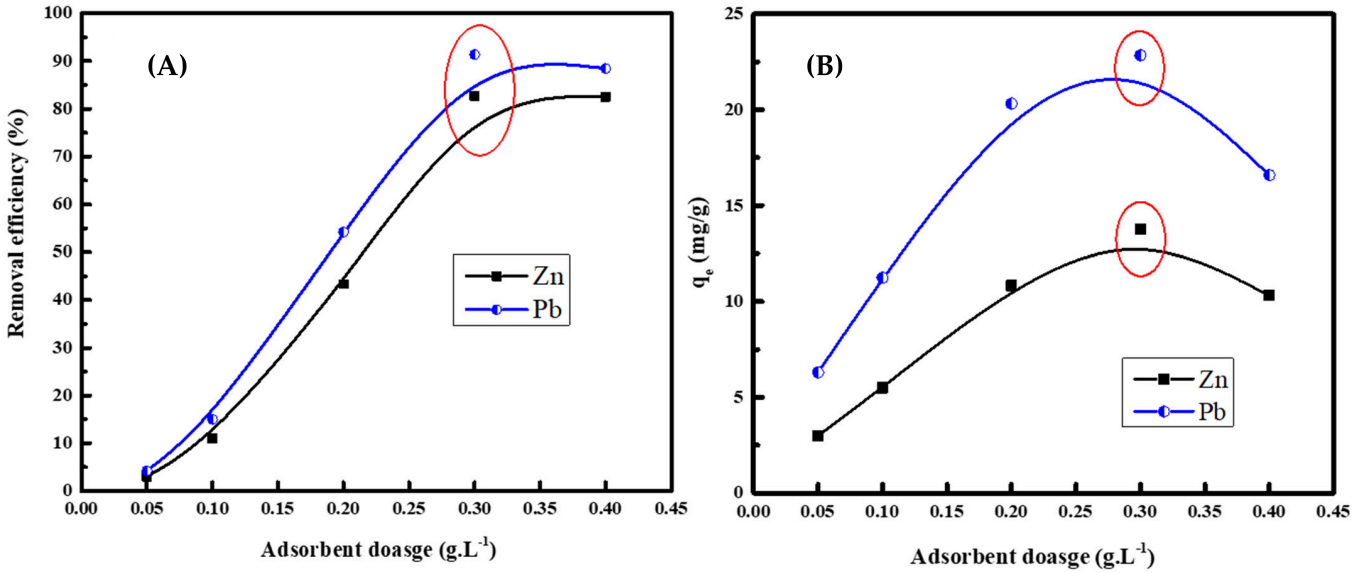


Figure 10. Effect of adsorbent dosage on heavy metal removal efficiency (**A**) and wood sawdust adsorption capacity (**B**).

3.2.4. Effect of Contact Time

Importantly, for a given starting concentration of the adsorbate, the adsorption kinetics of the adsorbent are reflected in the contact time. As illustrated in Figure 11A, the adsorption capacities for Zn^{2+} and Pb^{2+} metal ions rise significantly during the initial 60 min. of contact time. There are many empty binding sites and a lot of surface area in sawdust; therefore, when the metal ion adsorption capacity increases, it is due to these two factors. Zn and Pb removal efficiencies (R.E.) increase exponentially with increasing contact time from 10 to 60 min. At 10 min, the removal effectiveness for Zn is 46.8%; at 60 min, it improves to 97.92%; and at 10 min, it increases to 98.08% for Pb. With longer contact times, Pb and Zn concentrations in the treated synthetic model solutions eventually drop. These findings suggest that adsorbent-water contact duration is a key variable in Pb and Zn removal efficiency. This is most likely because there are more surface sites available for heavy metal ions adsorbed onto the adsorbent, allowing more ions to permeate into the porous structure [13]. After 60 min of contact time, heavy metals from synthetic model solutions were most effectively separated.

Accurately evaluating the sorption process requires the kinetic data that are collected. Equations (10)–(12), which are pseudo-first-order [71], pseudo-second-order [72], and intra-particle diffusion models [73], respectively, were used to assess the adsorption kinetics and determine the rate-controlling processes in the current investigation. These models formed the basis for the analysis of the experimental data, which led to the following conclusions:

Pseudo-first-order model:

$$\ln (q_e - q_t) = \ln q_e - k_1 t \quad (10)$$

Pseudo-second-order model:

$$\frac{t}{q_t} = \frac{1}{k_2 q_e^2} + \frac{t}{q_e} \quad (11)$$

Intra-particle diffusion model:

$$q_t = K_{DM}\, t^{0.5} + C \quad (12)$$

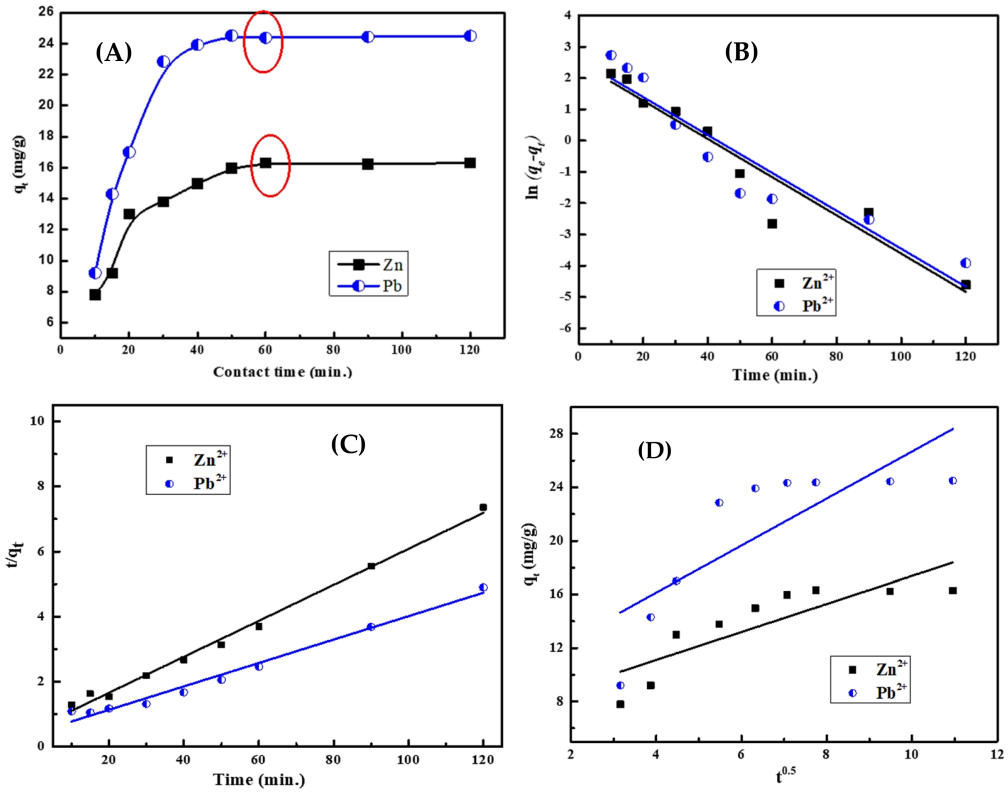


Figure 11. Effect of contact time on Zn^{2+} and Pb^{2+} adsorption capacity: (**A**) pseudo-first-order, (**B**) pseudo-second-order (**C**), and intra-particle diffusion (**D**).

In this study, the variables q_e and q_t (mg·g^{-1}) represent the amounts of heavy metal ions adsorbed at equilibrium and at a specific reaction time (in minutes), respectively. The parameters k_1 (min^{-1}), k_2 (g·mg^{-1}·min^{-1}), and K_{DM} (mg·g^{-1}·min$^{1/2}$) denote the rate constants for various kinetic models, while C signifies the boundary layer thickness. The slope and interception from the linear plot of ln (q_e–q_t) vs. time (t) were utilized to determine k_1 and q_{ecal} for the pseudo-first-order model, as presented in Figure 11B. Similarly, the equilibrium adsorption amount q_{ecal} and the pseudo-second-order rate constant (k_2) were calculated from the slope and intercept of the plot of t/q_t against time (t), as presented in Figure 11C. The intra-particle diffusion rate constant k_{md} and the correlation coefficient R^2 were derived from the straight-line plots of $q_t$vs.$t^{0.5}$, as presented in Figure 11D. The parameters for the several kinetic models considered are listed in Table 5. With an R^2 value of 0.98 or higher, the pseudo-second-order model provides the best fit to the sorption kinetics, according to the data. Moreover, the equilibrium adsorption capacities q_{ecal} computed using the pseudo-second-order model showed better agreement with the experimental values q_{eexp}. In terms of metal ion adsorption onto wood sawdust, this suggests a pseudo-second-order adsorption mechanism. It suggests that valence forces, which allow the adsorbate and adsorbent to share electrons, mostly affect chemisorption, the regulating phase in the adsorption method [35,74,75].

Table 5. Comparison of kinetic rate constants from pseudo-first-order, pseudo-second-order, and intraparticle diffusion models using experimental data; R^2 values imply effective kinetic model fit.

Metal Ions	Experimental Data	Pseudo-First-Order			Pseudo-Second-Order			Intra-Particle Diffusion		
	$q_{e,exp}$/ (mg·g^{-1})	$q_{e,cal}$/ (mg·g^{-1})	K_1/ (min^{-1})	R^2	$q_{e,cal}$/(mg·g^{-1})	K_2/ (g·mg^{-1} min^{-1})	R^2	K_{DM}/ (mg·g^{-1}·min$^{1/2}$)	C	R^2
Zn^{2+}	16.32	12.2	0.06	0.92	16.7	0.01	0.993	1.05	6.92	0.72
Pb^{2+}	24.52	14.15	0.06	0.891	27.7	0.0032	0.984	0.727	9.11	0.648

3.2.5. Effect of Initial Concentration

Figure 12A shows how the adsorption effectiveness of wood sawdust changes with various starting amounts of heavy metal ions. A consistent adsorbent dose of 0.3 g·L^{-1} was used throughout the experiment, with concentrations ranging from 10 to 80 ppm (mg·L^{-1}).

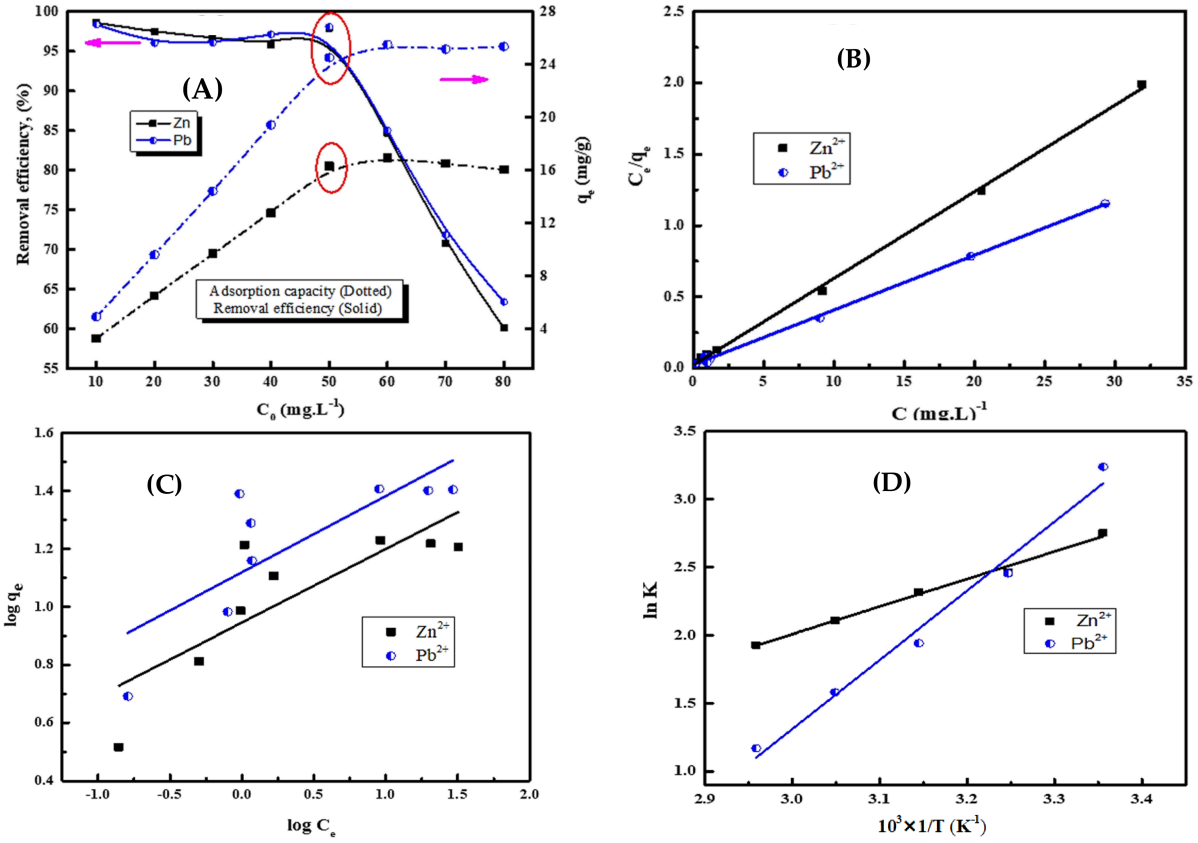


Figure 12. Effect of initial concentration on adsorption of Zn^{2+} and Pb^{2+} onto wood sawdust (**A**), Langmuir model (**B**), Freundlich model (**C**) and adsorption thermodynamic model (**D**).

The efficiency of metal ion removal decreases dramatically with increasing starting concentration. Figure 12A shows that the removal efficiencies for Pb and Zn are 98.39% and 98.61%, respectively, at the lowest initial concentration of 10 ppm, but these efficiencies tend to decline as the initial concentration increases at an adsorption temperature of 25 °C. Because the adsorbent surface has a limited number of adsorption sites, it remained stable with minimal change at concentrations above 50 mg·L^{-1} [74].

The findings show that the sawdust adsorbent has limited adsorption capacity and that removal effectiveness decreases with increasing initial heavy metal concentrations. This is probably because, as metal loadings increase, the adsorbent surface's accessible adsorption sites become saturated [74]. To remove Zn^{2+} and Pb^{2+} via adsorption, our results confirm that the accessibility of sites on wood sawdust is crucial. A removal efficiency of 98.08%

for Zn and 97.92% for Pb was achieved at a concentration of 50 ppm, the optimal level for heavy metal separation from prepared synthetic model solutions.

The Freundlich, Langmuir, and Temkin models, described by Equations (13)–(15), are among the models proposed to describe the adsorption isotherms of Zn^{2+} and Pb^{2+} onto wood sawdust.

Langmuir isotherm equation;

$$\frac{C_e}{q_e} = \frac{1}{q_{max}\, k_L} + \frac{C_e}{q_e} \tag{13}$$

Freundlich isotherm equation

$$logq_e = logK_F + \frac{1}{n}\, logC_e \tag{14}$$

Temkin isotherm equation

$$q_e = B_T\, ln\, k_T + B_T\, lnC_e \tag{15}$$

where C_e ($mg{\cdot}L^{-1}$) denotes the equilibrium concentration of metal ions adsorbed, q_e ($mg{\cdot}g^{-1}$), and q_{max} ($mg{\cdot}g^{-1}$) is the maximum amount of adsorption for a monolayer of the adsorbent. The Langmuir equilibrium adsorption constant k_L ($L{\cdot}mg^{-1}$) is derived from the linear plots of C_e/q_e vs. C_e , as illustrated in Figure 12B. Figure 12C shows the linear plots of $\log q_e$ vs. $\lg qC_e$, which are used to calculate the Freundlich adsorption isotherm constants, k_F ($mg{\cdot}g^{-1}$) and $1/n$, respectively, which represent the adsorbent's adsorption capacity and the adsorption process's heterogeneity. Finally, the binding energy at equilibrium B_T ($KJ{\cdot}mol^{-1}$) and the heat of adsorption K_T ($L{\cdot}g^{-1}$) are associated with each other.

Equilibrium data calculated from many linked equations are shown in Table 6. In comparison to alternative adsorption isotherm models, the data show that the Langmuir isotherm has the greatest correlation coefficients (R^2) for Zn^{2+} and Pb^{2+}, at 0.999 and 0.998, respectively. According to these numbers, the Langmuir model fits the experimental data best, indicating that its assumptions better describe the adsorption of the two metal ions onto the adsorbent. One way to find out whether the adsorption system is good is to use the dimensionless separation factor (R_L). It can be calculated using Equation (16) [47].

$$R_L = \frac{1}{1 + K_L C_0} \tag{16}$$

where C_0 denotes the initial concentration of metal ions ($mg{\cdot}L^{-1}$), whereas k_L signifies the Langmuir constant. Zn^{2+} ions have an R_L value of 0.00469, and Pb^{2+} ions have an R_L value of 0.00766, both of which are in the range $0 < R_L < 1$. These results show that, under all tested circumstances, the metal ion adsorption process onto the adsorbents is beneficial [76,77]. Key to understanding the binding energy between the solute and adsorbent, the Langmuir constant k_L reflects the spontaneity of the adsorption process. A more stable product with a larger adsorption capacity result from a more spontaneous adsorption process, as indicated by a higher k_L value. It seems that Zn^{2+} and Pb^{2+} may be readily adsorbed due to the relatively unstable adsorption of the two metal ions onto the adsorbent, as shown by the low k_L value observed in this work [69]. Thus, according to these results, the adsorption of lead ions (Pb^{2+}) and zinc ions (Zn^{2+}) occurs on the material's surface via heterogeneous chemical adsorption at comparable adsorption energies. As a result, the adsorption process is best described by the Langmuir isotherm model.

Table 6. Modeling of adsorption isotherms for the uptake of metal ions by wood sawdust; R^2 values indicate a well-fitted isotherm model.

Metal Ions	Langmuir				Freundlich			Temkin		
	$q_{e,cal}$/ (mg·g^{-1})	K_L / (L·mg^{-1})	R_L	R^2	K_F / (mg·g^{-1})/(mg·L^{-1})$^{1/n}$	$\frac{1}{n}$	R^2	B_T J·mol^{-1}	K_T (L·m^{-1})	R^2
Zn^{2+}	16.39	2.65	0.0046	0.999	8.912	4	0.67	2.31	88.66	0.71
Pb^{2+}	25.64	1.62	0.0076	0.998	13.18	3.78	0.63	3.67	60.57	0.67

Table 7 compares the findings of this investigation with those of earlier studies on the adsorption capacity of wood sawdust adsorbents for heavy metal ions. It was shown that the sawdust derived from softwood had a comparable adsorption capacity to other adsorbents and demonstrated a strong ability to remove various metals from prepared synthetic model solutions.

Table 7. A comparative analysis of several low cost-effective adsorbents for the adsorption of heavy metal ions.

Adsorbent	Adsorption Capacity q_{max} (mg·g^{-1})	Temp./°C	Ref.
Teakwood sawdust	11 (Cu^{2+}), 4.9 (Zn^{2+})	20	[78]
Picea smithiana sawdust	6.35 (Pb^{2+}), 2.87 (Cd^{2+})	25	[79]
Populus alba sawdust	10.125 (Pb^{2+}), 8.48 (Zn^{2+}), 8.87 (Cd^{2+})	25	[80]
Hornbeam sawdust	3.96 (Cu^{2+}), 4.4 (Zn^{2+})	30	[81]
Cherry sawdust	2.16 (Cu^{2+}), 1.46 (Zn^{2+})		
Poplar sawdust	3.88 (Cu^{2+}), 2.88 (Zn^{2+})		
Spruce sawdust (raw)	2.48 (Cu^{2+}), 2.01 (Zn^{2+})		
Meranti sawdust	32.1 (Cu^{2+}), 37.87 (Cr^{2+}), 35.9 (Ni^{2+}),34.24 (Pb^{2+})	30	[82]
Modified sawdust (Pinus sylvestris)	9.78 (Pb^{2+}), 9.29 (Cd^{2+})	25	[83]
Poplar sawdust (raw)	0.74 (Zn^{2+}), 0.86 (Cu^{2+})	20	[84]
Softwood sawdust	16.32 (Zn^{2+}), 24.52 (Pb^{2+})	25	This work

3.3. Adsorption Thermodynamics

The thermodynamic variables related to the effect of temperature on the adsorption mechanism of heavy metal ions were determined using Equations (17)–(20) to calculate entropy (ΔS°), enthalpy (ΔH°), and free energy change (ΔG°).

$$\Delta G^\circ = -RT\, lnK_c \tag{17}$$

$$K_d = \frac{q_e}{C_e} \tag{18}$$

$$\Delta G^\circ = \Delta H^\circ - T\Delta S^\circ \tag{19}$$

$$lnK_L = \frac{\Delta S^\circ}{R} - \frac{\Delta H^\circ}{RT} \tag{20}$$

where K_L is the Langmuir equilibrium constant, R is the universal gas constant (8.314 J·mol^{-1}K^{-1}), and T is the reaction temperature in Kelvin. It is possible to determine the values of ΔH° and ΔS° by analyzing the slope and intercept of a linear plot of ln k vs. 1/T, as shown in Figure 12D. The results obtained, along with the relevant thermodynamic data, are summarized in Table 8. These findings indicate that the adsorption process is exothermic, as the ΔH° values ranging from 298 to 338 K are negative. Moreover, it may be inferred that the adsorption process becomes less favorable as the temperature increases, based on the observed drop in K_L and the little change in the absolute value of $|\Delta G^\circ|$. At lower temperatures, the spontaneous and effective adsorption of Zn^{2+} and Pb^{2+} ions onto the sawdust adsorbent is more favorable, as indicated by the negative values of (ΔG°) and the standard entropy change (ΔS°). Also, there is less randomness at the solid–liquid interfaces when the adsorption process is underway [77].

Table 8. Values of thermodynamic parameters for Zn^{2+} and Pb^{2+}, adsorption upon wood sawdust, R^2 values suggest a well-fitted thermodynamic model.

Metal Ions	ΔH^0	ΔS^0	ΔG^0(KJ.mol^{-1})					R^2
	(KJ·mol^{-1})	(J·mol^{-1}K^{-1})	298 °K	308 °K	318 °K	328 °K	338 °K	
Zn^{2+}	−0.017	−33.75	−6.8211	−6.3079	−6.1267	−5.7425	−5.42036	0.99
Pb^{2+}	−0.092	−75.66	−6.0281	−6.2888	−5.1358	−4.31079	−3.28640	0.97

3.4. Mechanism of Adsorption Process

The surface morphology of sawdust was examined using SEM-EDX to determine its ability to adsorb heavy metal ions. Figure 13 shows that the porosity of wood cells is uneven. Pores and cracks in the cellular structure are clearly visible in certain areas. The main components of sawdust are carbon, oxygen, and hydrogen, with trace quantities of additional elements. It was observed that the surface of the sawdust becomes rough following the sorption of Zn^{2+} and Pb^{2+} ions, although the crystalline structure stays almost the same after the absorption process.

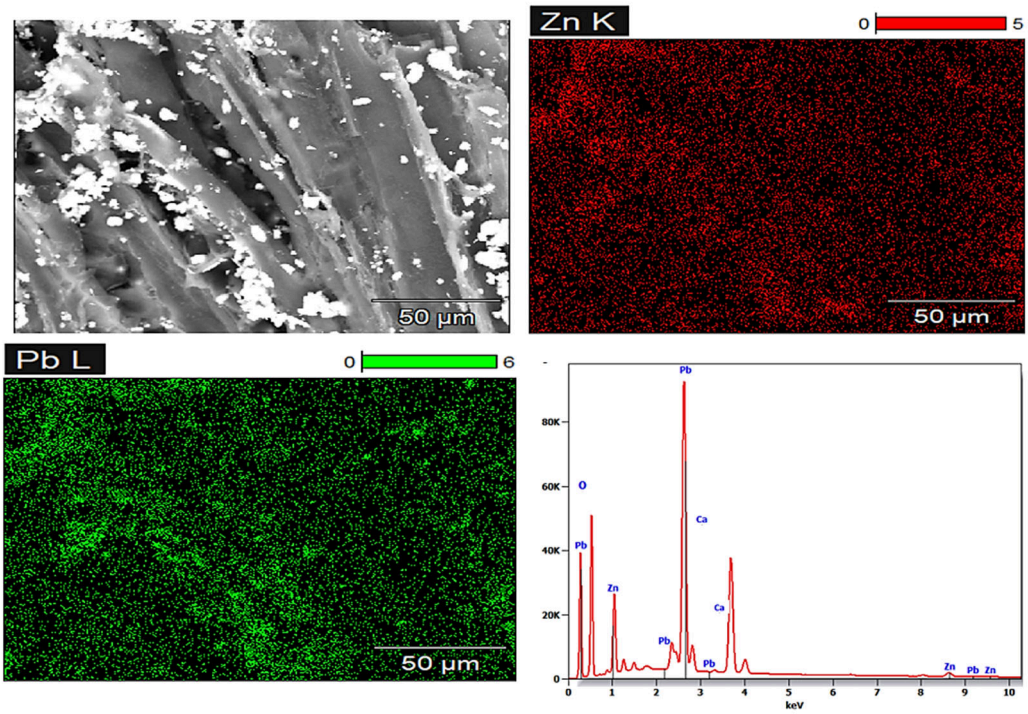


Figure 13. SEM analysis of the surface morphology and EDS after adsorption of Zn^{2+} and Pb^{2+}.

There is a prominent peak in the spectrum that can be seen at around 2.3 keV. This peak corresponds to the typical X-ray emission energy of lead. The presence of zinc in the sample is indicated by the existence of multiple minor peaks at around 8.6 keV and 1.0 keV, both of which are present. The entire intensity or quantity of the elemental composition identified in the sample is represented by the total full-scale count for the spectrum, which is 94.4 keV. A measurement of the entire signal strength over the entire spectrum may be obtained by calculating the total integral counts, which sum to 3878 keV. The presence of large peaks for lead and zinc in this EDX spectrum provides evidence that the sample under investigation contains a significant amount of both elements. There is information about the relative concentrations of these elements in the sample that may be gleaned from the respective strengths of these peaks.

The analysis of wood sawdust as a biosorbent for heavy metal ions such as Zn^{2+} and Pb^{2+} is crucial for understanding its efficiency and mechanisms in environmental

remediation. SEM-EDS offers insights into the morphology and elemental composition of the adsorbent before and after metal ion exposure as detailed in Figure 14. The SEM images may reveal changes in the surface structure of wood sawdust post-adsorption. These changes could indicate the binding sites that the metal ions have engaged, such as the formation of new surface features or a change in particle aggregation. EDS spectra should show an increase in the atomic percentages of Zn and Pb in the adsorbent after treatment. Species locations could help identify specific binding sites on the wood fibers or other structures where these ions were captured.

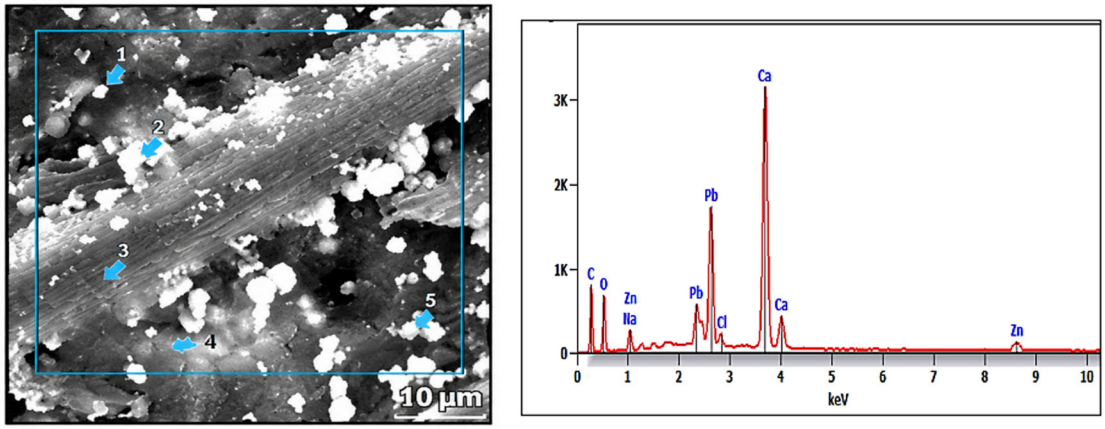


Figure 14. SEM-EDS analysis of wood sawdust post-adsorption of Zn^{2+} and Pb^{2+} at different locations.

By analyzing different locations on the sawdust sample (Table 9), variations in metal distribution can suggest the heterogeneity of adsorption. Areas with higher concentrations of adsorbed metals might correlate with particular structural features of wood sawdust. The interaction of heavy metals with wood sawdust involves functional groups on cell wall components such as cellulose, hemicellulose, and lignin. Post-adsorption analysis might indicate the involvement of these groups in binding Zn^{2+} and Pb^{2+}. The adsorption mechanism can also involve ion exchange, where metal ions replace other cations present in the wood sawdust, or complexation with free hydroxyl groups available on the wood surface. It is important to differentiate between physical adsorption (e.g., van der Waals forces) and chemical adsorption (e.g., covalent bonds). The EDS data may provide hints about which process predominates, depending on how firmly metals are held.

Table 9. Composition analysis of loaded wood samples from five different locations and stander deviation (S.D).

Locations	C	O	Na	Cl	Ca	Zn	Pb
location 1	23.9	36.4	2.8	12.5	15.8	2.2	6.6
location 2	28.5	29.5	2.1	15.3	15.9	2.6	6.1
location 3	14.7	26.7	2.0	11.4	28.7	3.6	12.9
location 4	15.2	32.4	2.2	10.3	24.5	4.0	11.4
location 5	15.5	26.1	2.6	11.3	29.5	3.7	11.2
S.D.	19.56	30.22	2.34	12.16	22.88	3.22	9.64

The sample is primarily composed of carbon (C), oxygen (O), calcium (Ca), sodium (Na), chlorine (Cl), lead (Pb), and zinc (Zn), as detailed in Table 8. The carbon content varies between 14.7% and 28.5%, while oxygen levels range from 20.1% to 36.4%. Calcium is present at 11.3% to 29.5%, sodium comprises 2.0% to 2.8%, and chlorine accounts for 10.3% to 15.8%. Additionally, lead concentrations range from 6.1% to 12.9%, and zinc levels fall between 2.2% and 3.7%.

By studying the surface chemistry of the wood sawdust adsorbent and its interactions with metal ions using X-ray photoelectron spectroscopy (XPS) (Axis Ultra DLD-600W,

Kratos, UK), we gained a better understanding of the adsorption process. Both the pre- and post-adsorption spectra of the sawdust surface are shown in Figure 15A. Figure 15B demonstrates that the adsorption of Zn^{2+} is validated by the appearance of new peaks at roughly 1021.8 eV and 1045.3 eV in the high-resolution spectra, corresponding to Zn2p3/2 and Zn2p1/2, respectively. The Na1s peak at around 1073.2 eV decreased significantly, indicating effective Zn^{2+} adsorption on the adsorbent's surface via ion exchange [85]. In addition, a peak at 124.35 eV indicates that there may be specific sites where Zn^{2+} may react with OH- groups to generate precipitation chemical compounds ($Zn(OH)_2$) on the sawdust's surface. Two separate peaks in the 138.9–143.8 eV region were seen after Pb^{2+} adsorption, as shown in Figure 15C. The peak at roughly 138.9 eV belongs to Pb4f7/2, and the peak at 143.8 eV is ascribed to Pb4f5/2. The findings suggest that Pb^{2+} binding to the adsorbent surface is governed by surface precipitation or by adsorption complexation [13,86].

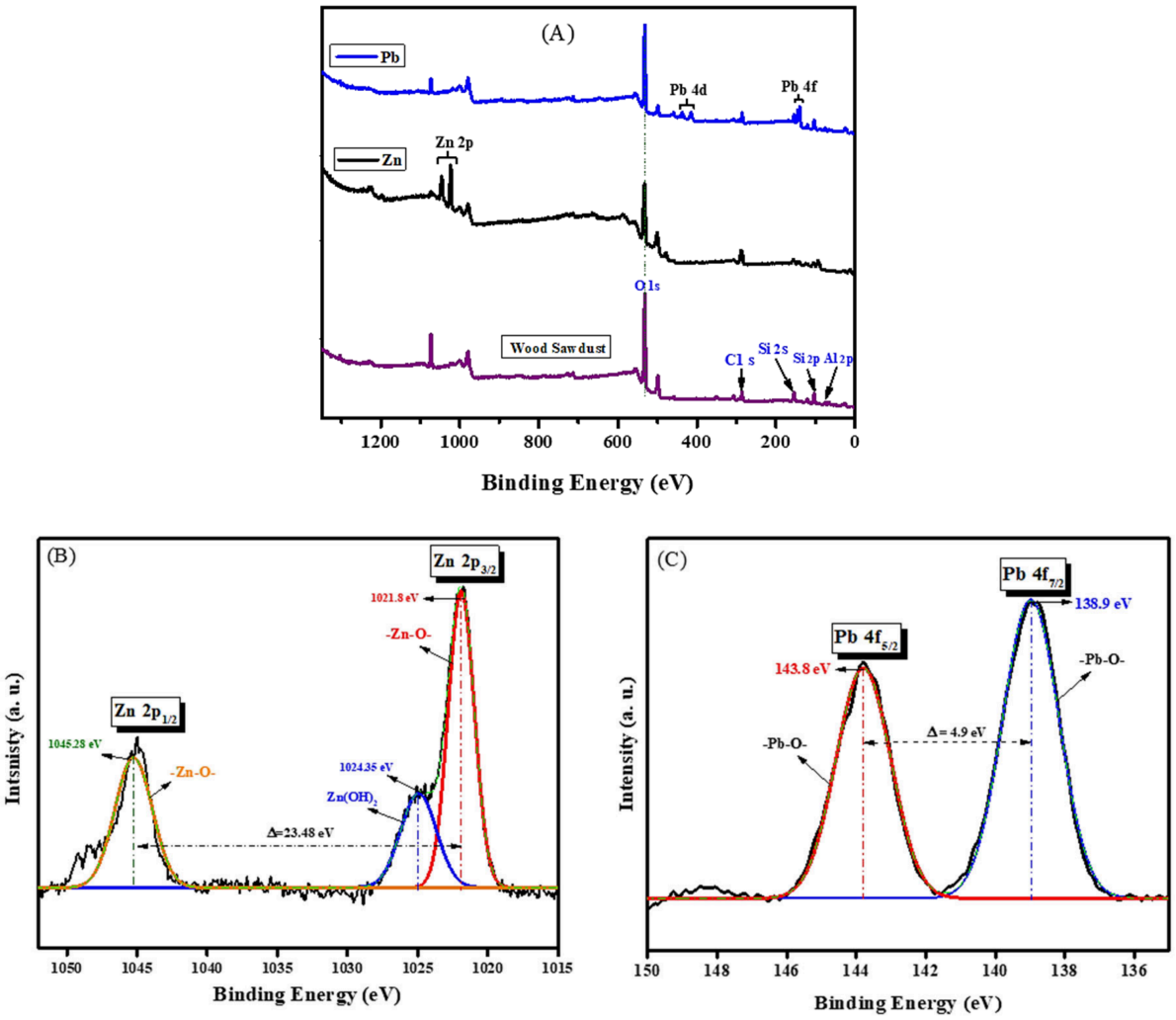


Figure 15. X-ray Photoelectron spectroscopy (XPS) wide scans of wood sawdust before and after Zn and Pb adsorption are shown full spectrum (**A**), high-resolution Zn2p spectrum (**B**), and high-resolution Pb4f spectrum (**C**).

Figure 16 depicts the hypothesized absorption process based on EDX and XPS findings. It suggests that electrostatic attraction, physical adsorption, and surface complexation are the three main phenomena involved in the adsorption of Zn^{2+} and Pb^{2+} on sawdust [69,87]. Complexation is the primary process by which Zn^{2+} is absorbed from aqueous solutions. The following Equation (21) describes the process:

(Wood sawdust based adsorbent) 2(X-OH) + Me^{2+} → (Wood sawdust based adsorbent)Me^{2+} (21)

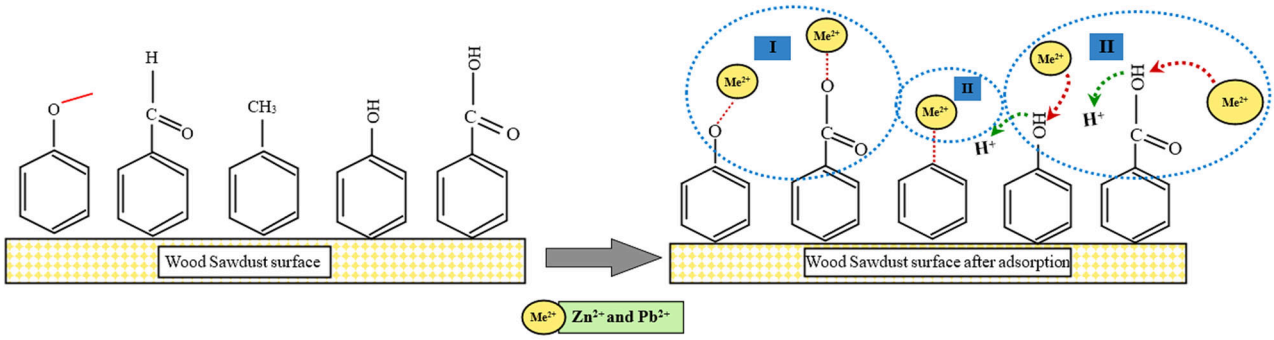


Figure 16. Proposed mechanism for the adsorption of heavy metal-ions onto the used sawdust, where I Electrostatic attraction, II physical adsorption III complexation ($(Me(OH)^+$).

3.5. Reusability and Desorption of Wood Sawdust (WS)

Figure 17 shows the process of reusing a heavy metal ion adsorbent made of sawdust by going through many adsorption–desorption cycles under ideal circumstances. In experimental settings, residual values remain below detection limits. Despite a slight decrease in performance over four cycles, the data show that wood sawdust retains good removal efficiencies for Zn and Pb ions. Thus, to establish a closed recycling process, the adsorbent must be cleaned once contaminants reach a certain enrichment level. The first cycle achieved a removal efficiency of about 98% for Pb and 96% for Zn. By the fourth cycle, the efficiencies for Zn were about 86%, and for Pb, 90.5%. It seems that wood sawdust retains its adsorption capacity even after repeated use, making it a good choice for long-term prepared synthetic model solutions treatment applications, as this minor loss in performance suggests [88].

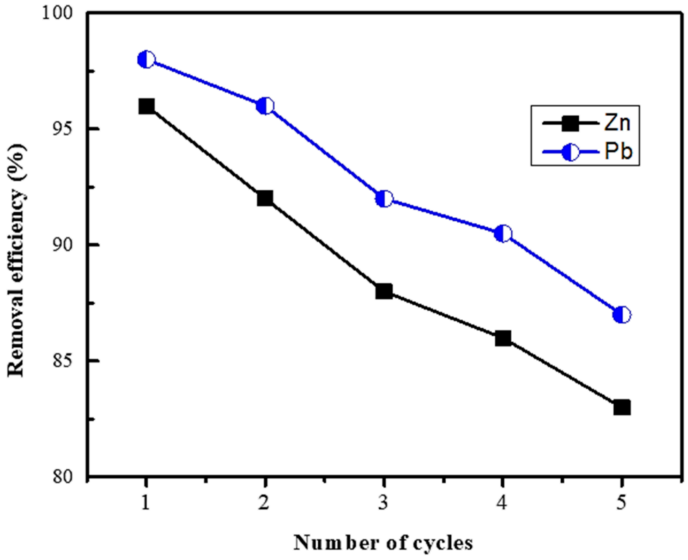


Figure 17. The adsorption efficiency of sawdust in relation to the number of cycles under optimal conditions.

The steady loss of active functional groups, particularly hydroxyl (OH^-) groups, on the surface of the wood sawdust adsorbent is primarily responsible for the significant decrease in adsorption effectiveness observed across multiple cycles. The chemisorption and physisorption processes, which are crucial for heavy metal removal from prepared

synthetic model solutions, rely on these functional groups. The accessible binding sites for metal ions likely became saturated or degraded as the number of adsorption cycles increased. The regeneration procedure, which included desorption with 0.1 M HCl, may also have worn down the adsorbent surface to some extent, which would explain why its adsorption capacity gradually decreased. Past studies [52,78,89] have shown that adsorbents may undergo structural changes and lose active sites after prolonged exposure to acidic environments, findings that are consistent with our current findings.

3.6. Treatment of the Industrial Effluent Sample from EGPC

Table 10 shows the pre-and post-adsorption concentrations of heavy metal ions that were targeted using softwood sawdust. Recommendations for wastewater drainage from the World Health Organization (WHO) are used to compare the concentrations [50]. The effluent sample obtained from the Egyptian General Petroleum Corporation (EGPC) contains zinc and lead, which are the most important elements under drainage water laws. Except for Mn (0.64 $mg{\cdot}L^{-1}$) and Fe (3.1 $mg{\cdot}L^{-1}$) in the first cycle, all residual values within the experimental setup are consistently below the detection limits. Nevertheless, after the fourth adsorption cycle, the remaining amounts of heavy metal ions comply with the World Health Organization's standards for the effective disposal of wastewater in marine environments [49]. Heavy metal ions in wastewater rise with 4th-cycle circulations. Adsorption is inhibited by co-contaminants competing for active sites, blocking pores, altering surface charge, or generating soluble metal–organic complexes [52]. Once impurities are enriched, the adsorbent must be cleaned for closed recycling. Sawdust may safeguard industrial wastewater drainage as a last stage.

Table 10. Utilization of sawdust for the extraction of heavy metal ions from EGPC industrial effluent samples.

Metals		Cd	Cr	Cu	Mn	Pb	Fe	Ni	Zn
C_0 ($mg{\cdot}L^{-1}$)		0.001	0.001	0.1	0.64	17.6	0.04	0.002	12.5
MLD $_{WHO}$		0.01	0.01	1	0.1	0.01	1.5	0.1	1
Number of Cycles	1	U.D.	U.D.	U.D.	U.D.	U.D.	U.D.	U.D.	U.D.
	2	U.D.	U.D.	U.D.	U.D.	U.D.	U.D.	U.D.	U.D.
	3	U.D.	U.D.	U.D.	U.D.	5.7	U.D.	U.D.	4
	4	0.41	0.28	0.3	0.4	5.9	1.2	0.054	8

C_0($mg{\cdot}L^{-1}$): Concentration of heavy metal ions in wastewater from EGPC; U.D.: Under detection limit; MLD $_{WHO}$: Maximum WHO wastewater disposal limits.

4. Conclusions

This study investigates the potential of wood sawdust as an eco-friendly, cost-effective adsorbent for the treatment of prepared synthetic model solutions, specifically focusing on the removal of heavy metal ions, including zinc (Zn^{2+}) and lead (Pb^{2+}). The results indicate that wood sawdust exhibits remarkable adsorption capacities, achieving removal efficiencies of 98.2% for Zn and 98.1% for Pb under optimal conditions. Key factors influencing adsorption, including particle size, pH, adsorbent dosage, and contact time, were thoroughly evaluated and optimized, resulting in significant improvements in metal ion removal. Also tested was wood sawdust's regenerative capacity, with results showing a steady decrease in adsorption effectiveness across multiple cycles. The primary reason for this reduction is the absence of metal-ion-binding active functional groups on the adsorbent surface. Reusing sawdust showed promise; however, the efficiency decreased with each cycle owing to possible deterioration during regeneration. The findings underscore the viability of wood sawdust as a sustainable alternative for removing heavy metals from wastewater, contributing to environmental conservation and resource recycling. However,

to enhance the long-term usability of wood sawdust as an adsorbent, future research should explore methods to improve its stability and adsorption performance, including surface modifications and the implementation of various regeneration strategies. Overall, this study highlights the importance of using natural and renewable materials for industrial wastewater treatment, aligning with global sustainability goals. Detailed investigation on regeneration techniques and surface modifications is recommended to improve the long-term performance of this natural adsorbent in wastewater applications.

Author Contributions: Conceptualization, G.S.A., M.A.E., A.H.I. and A.B.E.; Methodology, G.S.A., M.A.E., A.H.I. and A.B.E.; Software, G.S.A., M.A.E., A.H.I. and A.B.E.; Validation, A.H.I. and A.B.E.; Formal analysis, A.H.I. and A.B.E.; Investigation, G.S.A., M.A.E., A.H.I. and A.B.E.; data curation, A.H.I. and A.B.E.; Writing—original draft preparation, A.H.I. and A.B.E.; Writing—review and editing, G.S.A., M.A.E., A.H.I. and A.B.E.; Visualization, A.H.I. and A.B.E.; Supervision, G.S.A. and A.B.E.; Project administration, G.S.A.; Funding acquisition, G.S.A. All authors have read and agreed to the published version of the manuscript.

Funding: This project was funded by The Deanship of Scientific Research (DSR) at King Abdulaziz University, Jeddah, Saudi Arabia under grant no. (IPP:604-135-2025). The authors, therefore, acknowledge with thanks DSR for technical and financial support.

Institutional Review Board Statement: Not applicable.

Informed Consent Statement: Not applicable.

Data Availability Statement: The original contributions presented in this study are included in the article. Further inquiries can be directed to the corresponding author.

Acknowledgments: The authors express their gratitude for the financial support that was received through grants from The Deanship of Scientific Research (DSR) at King Abdulaziz University, Jeddah, Saudi Arabia provide funding for this study under grant number (IPP:604-135-2025). The authors, therefore, acknowledge with thanks DSR for technical and financial support.

Conflicts of Interest: The authors declare no conflicts of interest.

References

1. AbuZeid, K.; Elrawady, M. *Strategic Vision 2030 for Treated Wastewater Reuse in Egypt*; CEDARE: Cairo, Egypt, 2014; pp. 1–48.
2. Hellal, M.S.; Al-Sayed, A.; El-Liethy, M.A.; Hassan, G.K. Technologies for Wastewater Treatment and Reuse in Egypt: Prospectives and Future Challenges. In *Handbook of Advanced Approaches Towards Pollution Prevention and Control*; Elsevier: Amsterdam, The Netherlands, 2021; Volume 2, pp. 275–310. [CrossRef]
3. El-Gamal, T.T.; Housian, M.H. Wastewater Challenges and the Successful Implementation of Constructed Wetlands in Egypt (Egypt). *Safe Use Wastewater Agric. Good Pract. Ex.* **2018**, *1*, 21–26.
4. Abdallah, M.N. Wastewater Operation and Maintenance in Egypt (Specific Challenges and Current Responses). *Int. J. Sci. Basic Appl. Res.* **2014**, *18*, 125–142.
5. El Monayeri, D.S.; El Monayeri, O.D.; El Gohary, E.H.; Aboul-fotoh, A.M. Industrial Wastewater Treatment Systems in Egypt: Difficulties and Proposed Solutions. In *Security of Industrial Water Supply and Management*; Springer: Berlin/Heidelberg, Germany, 2011; pp. 209–230.
6. Bao, W.; Zou, H.; Gan, S.; Xu, X.; Ji, G.; Zheng, K. Adsorption of Heavy Metal Ions from Aqueous Solutions by Zeolite Based on Oil Shale Ash: Kinetic and Equilibrium Studies. *Chem. Res. Chin. Univ.* **2013**, *29*, 126–131. [CrossRef]
7. Hamadi, A.; Nabih, K. Synthesis of Zeolites Materials Using Fly Ash and Oil Shale Ash and Their Applications in Removing Heavy Metals from Aqueous Solutions. *J. Chem.* **2018**, *2018*, 6207910. [CrossRef]
8. Meng, J.; Cui, J.; Yu, J.; Huang, W.; Wang, P.; Wang, K.; Liu, M.; Song, C.; Chen, P. Preparation of Green Chelating Fibers and Adsorption Properties for Cd(II) in Aqueous Solution. *J. Mater. Sci.* **2018**, *53*, 2277–2289. [CrossRef]
9. Mofarrah, A.; Husain, T.; Chen, B. Optimizing Cr(VI) Adsorption on Activated Carbon Produced from Heavy Oil Fly Ash. *J. Mater. Cycles Waste Manag.* **2014**, *16*, 482–490. [CrossRef]
10. Wang, X.S.; Miao, H.H.; He, W.; Shen, H.L. Competitive Adsorption of Pb(II), Cu(II), and Cd(II) Ions on Wheat-Residue Derived Black Carbon. *J. Chem. Eng. Data* **2011**, *56*, 444–449. [CrossRef]

11. Yu, Z.; Dang, Q.; Liu, C.; Cha, D.; Zhang, H.; Zhu, W.; Zhang, Q.; Fan, B. Preparation and Characterization of Poly(Maleic Acid)-Grafted Cross-Linked Chitosan Microspheres for Cd(II) Adsorption. *Carbohydr. Polym.* **2017**, *172*, 28–39. [CrossRef] [PubMed]
12. Cheng, Q.; Huang, Q.; Khan, S.; Liu, Y.; Liao, Z.; Li, G.; Ok, Y.S. Adsorption of Cd by Peanut Husks and Peanut Husk Biochar from Aqueous Solutions. *Ecol. Eng.* **2016**, *87*, 240–245. [CrossRef]
13. Chen, G.; Shah, K.J.; Shi, L.; Chiang, P.C. Removal of Cd(II) and Pb(II) Ions from Aqueous Solutions by Synthetic Mineral Adsorbent: Performance and Mechanisms. *Appl. Surf. Sci.* **2017**, *409*, 296–305. [CrossRef]
14. Dupont, L.; Guillon, E. Removal of Hexavalent Chromium with a Lignocellulosic Substrate Extracted from Wheat Bran. *Environ. Sci. Technol.* **2003**, *37*, 4235–4241. [CrossRef] [PubMed]
15. U.S. Department of Health and Human Services; AWWAO. *Drinking Water Advisory Communication Toolbox—2016*; CDC: Atlanta, GA, USA, 2016.
16. Alcântara, R.R.; Muniz, R.O.R.; Fungaro, D.A. Full Factorial Experimental Design Analysis of Rhodamine B Removal from Water Using Organozeolite from Coal Bottom Ash. *Int. J. Energy Environ.* **2016**, *7*, 357–374. [CrossRef]
17. Valentukeviciene, M.; Andriulaityte, I.; Karczmarczyk, A.; Zurauskiene, R. Removal of Residual Chlorine from Stormwater Using Low-Cost Adsorbents and Phytoremediation. *Environments* **2024**, *11*, 101. [CrossRef]
18. Rashed, M.N. Adsorption Technique for the Removal of Organic Pollutants from Water and Wastewater. *Org. Pollut.—Monit. Risk Treat.* **2013**, *1*, 167–194. [CrossRef] [PubMed]
19. Matilainen, A.; Vepsäläinen, M.; Sillanpää, M. Natural Organic Matter Removal by Coagulation during Drinking Water Treatment: A Review. *Adv. Colloid Interface Sci.* **2010**, *159*, 189–197. [CrossRef] [PubMed]
20. Visa, M.; Isac, L.; Duta, A. Fly Ash Adsorbents for Multi-Cation Wastewater Treatment. *Appl. Surf. Sci.* **2012**, *258*, 6345–6352. [CrossRef]
21. USEPA (United States Environmental Protection Agency). *EPA Guidlines for Water Reuse, 2012; Guidelines for Water Reuse 600/R 12/618*; USEPA: Washington, DC, USA, 2012; 643p.
22. Torres-Castañón, L.A.; Robledo-Peralta, A.; Antileo, C.; Silerio-Vázquez, F.d.J.; Proal-Nájera, J.B. Sawdust-Based Adsorbents for Water Treatment: An Assessment of Their Potential and Challenges in Heavy Metal Adsorption. *J. Hazard. Mater. Adv.* **2025**, *18*, 100758. [CrossRef]
23. García-Flores, A.; Gutiérrez-Paredes, G.J.; Merchán-Cruz, E.A.; Zacarías, A.; Flores-Herrera, L.A.; Sandoval-Pineda, J.M. Review of Wood Sawdust Pellet Biofuel: Preliminary SWOT and CAME Analysis. *Processes* **2025**, *13*, 3607. [CrossRef]
24. Akhtar, M.; Sarfraz, M.; Ahmad, M.; Raza, N.; Zhang, L. Use of Low-Cost Adsorbent for Waste Water Treatment: Recent Progress, New Trend and Future Perspectives. *Desalin. Water Treat.* **2025**, *321*, 100914. [CrossRef]
25. Meez, E.; Rahdar, A.; Kyzas, G.Z. Sawdust for the Removal of Heavy Metals from Water: A Review. *Molecules* **2021**, *26*, 4318. [CrossRef] [PubMed]
26. Shaheen, S.M.; Eissa, F.I.; Ghanem, K.M.; El-Din, H.M.G.; Anany, F.S. Al Metal Ion Removal from Wastewaters by Sorption on Activated Carbon, Cement Kiln Dust, and Sawdust. *Water Environ. Res.* **2015**, *87*, 506–515. [CrossRef] [PubMed]
27. Sui, C.; Xie, W.; Bian, Y.; Li, X. Recent Progress in Adsorption Removal of Heavy Metal Ions from Wastewater Using Biomass-Based Materials. *Gels* **2026**, *12*, 311. [CrossRef] [PubMed]
28. Pertiwi, B.C.; Firginia, N.; Satyasyauqi, M.F.; Matovanni, M.P.N. Comparative Analysis of Biomass-Based Adsorbents for Heavy Metal Ion Removal. *Int. J. Eco-Innov. Sci. Eng.* **2025**, *6*, 30–37. [CrossRef]
29. Das, J.; Mondal, A.; Nag, S. Mechanistic Insights into the Competitive Sequestration of Cd^{2+}, Pb^{2+} and Ni^{2+} on KOH-Impregnated Hevea Brasiliensis Sawdust Activated Carbon. *Int. J. Environ. Anal. Chem.* **2025**, *106*, 2057–2084. [CrossRef]
30. Elboughdiri, N.; Azeem, B.; Ghernaout, D.; Ghareba, S.; Kriaa, K. Steam-Activated Sawdust Efficiency in Treating Wastewater Contaminated by Heavy Metals and Phenolic Compounds. *Water Reuse* **2021**, *11*, 391–409. [CrossRef]
31. Das, J.; Mondal, A.; Nag, S. Competitive Sequestration Behavior and Mechanism of Cd^{2+}, Pb^{2+} and Ni^{2+} Ions from Single, Binary and Ternary Metal Laden Solution by Hevea Brasiliensis Wood Sawdust (HBS). *J. Dispers. Sci. Technol.* **2025**, *46*, 2065–2078. [CrossRef]
32. Memon, S.Q.; Memon, N.; Shah, S.W.; Khuhawar, M.Y.; Bhanger, M.I. Sawdust—A Green and Economical Sorbent for the Removal of Cadmium (II) Ions. *J. Hazard. Mater.* **2007**, *139*, 116–121. [CrossRef] [PubMed]
33. Lavrova, S.; Yavorov, N. Potential of Wood Processing Residues as Eco-Friendly Adsorbents for Wastewater Treatment. *Materials* **2026**, *19*, 578. [CrossRef] [PubMed]
34. Al-Labadi, I.G.; Horváth, M.; Alkilani, A.T.; Al-Ma'abreh, A.M.; Bashir, M.J.K.; Keshta, B.E.; Hanbali, G.; Al Zoubi, W.; Abukhadra, M.R.; Alqhtani, H.A.; et al. Simultaneous Adsorptive Removal of Pb^{2+}, Cd^{2+}, Cu^{2+}, and Zn^{2+} Using Raw Norway Spruce Biomass: A Low-Cost and Eco-Friendly Solution for Wastewater Treatment. *Front. Water* **2025**, *7*, 1612232. [CrossRef]
35. Tejada-Tovar, C.; Villabona-Ortíz, A.; Ortega-Toro, R.; Mancilla-Bonilla, H.; Espinoza-León, F. Potential Use of Residual Sawdust of Eucalyptus Globulus Labill in Pb (II) Adsorption: Modelling of the Kinetics and Equilibrium. *Appl. Sci.* **2021**, *11*, 3125. [CrossRef]

36. Duong, T.M.H.; Van, H.-T.; Tran, T.P.; Nguyen, D.H.; Luu, T.C.; Do, D.A.; Nguyen, T.B.H.; Nga Luong, T.Q. Ozone-Functionalized Acacia Wood Sawdust Biochar for Total Nitrogen Adsorption from Pig Wastewater. *Mater. Res. Express* **2025**, *12*, 125502. [CrossRef]
37. Issaka, S.A.; Abdurahman, H.N.; Rosli, Y.M. Review on the Fundamental Aspects of Petroleum Oil Emulsions and Techniques of Demulsification. *J. Pet. Environ. Biotechnol.* **2015**, *6*, 1000214. [CrossRef]
38. Zolfaghari, R.; Fakhru'l-Razi, A.; Abdullah, L.C.; Elnashaie, S.S.E.H.; Pendashteh, A. Demulsification Techniques of Water-in-Oil and Oil-in-Water Emulsions in Petroleum Industry. *Sep. Purif. Technol.* **2016**, *170*, 377–407. [CrossRef]
39. Dejam, M.; Hassanzadeh, H.; Chen, Z. A Reduced-Order Model for Chemical Species Transport in a Tube with a Constant Wall Concentration. *Can. J. Chem. Eng.* **2018**, *96*, 307–316. [CrossRef]
40. Kang, W.; Yin, X.; Yang, H.; Zhao, Y.; Huang, Z.; Hou, X.; Sarsenbekuly, B.; Zhu, Z.; Wang, P.; Zhang, X.; et al. Demulsification Performance, Behavior and Mechanism of Different Demulsifiers on the Light Crude Oil Emulsions. *Colloids Surf. A Physicochem. Eng. Asp.* **2018**, *545*, 197–204. [CrossRef]
41. Yi, M.; Huang, J.; Wang, L. Research on Crude Oil Demulsification Using the Combined Method of Ultrasound and Chemical Demulsifier. *J. Chem.* **2017**, *2017*, 9147926. [CrossRef]
42. Mhatre, S.; Simon, S.; Sjöblom, J.; Xu, Z. Demulsifier Assisted Film Thinning and Coalescence in Crude Oil Emulsions under DC Electric Fields. *Chem. Eng. Res. Des.* **2018**, *134*, 117–129. [CrossRef]
43. Sun, N.; Jiang, H.; Wang, Y.; Qi, A.A. A Comparative Research of Microwave, Conventional-Heating, and Microwave/Chemical Demulsification of Tahe Heavy-Oil-in-Water Emulsion. *SPE Prod. Oper.* **2018**, *33*, 371–381.
44. Nikkhah, M.; Tohidian, T.; Rahimpour, M.R.; Jahanmiri, A. Efficient Demulsification of Water-in-Oil Emulsion by a Novel Nano-Titania Modified Chemical Demulsifier. *Chem. Eng. Res. Des.* **2015**, *94*, 164–172. [CrossRef]
45. Daniel-David, D.; Le Follotec, A.; Pezron, I.; Dalmazzone, C.; Noïk, C.; Barré, L.; Komunjer, L. Destabilisation of Water-in-Crude Oil Emulsions by Silicone Copolymer Demulsifiers. *Oil Gas. Sci. Technol.* **2008**, *63*, 9–19. [CrossRef]
46. Abdurahman, N.H.; Rosli, Y.M.; Azhari, N.H.; Hayder, B.A. Pipeline Transportation of Viscous Crudes as Concentrated Oil-in-Water Emulsions. *J. Pet. Sci. Eng.* **2012**, *90–91*, 139–144. [CrossRef]
47. Çalik, P.; Çalik, G.; Özdamar, T.H. Oxygen-Transfer Strategy and Its Regulation Effects in Serine Alkaline Protease Production by Bacillus Licheniformis. *Biotechnol. Bioeng.* **2000**, *69*, 301–311. [CrossRef]
48. Zhang, Y.; Gao, B.; Lu, L.; Yue, Q.; Wang, Q.; Jia, Y. Treatment of Produced Water from Polymer Flooding in Oil Production by the Combined Method of Hydrolysis Acidification-Dynamic Membrane Bioreactor-Coagulation Process. *J. Pet. Sci. Eng.* **2010**, *74*, 14–19. [CrossRef]
49. WHO (World Health Organization). Guidelines for the Safe Use of Wastewater, Excreta and Greywater. In *Wastewater Use in Agriculture*; World Health Organization: Geneva, Switzerland, 2006; Volume 2.
50. The Egyptian Environmental Affairs Agency (EEAA). *National Network for Monitoring Ambient Air Pollutants*; The Egyptian Environmental Affairs Agency (EEAA): Cairo, Egypt, 2015.
51. Liu, M.; Hou, L.-A.; Xi, B.; Zhao, Y.; Xia, X. Synthesis, Characterization, and Mercury Adsorption Properties of Hybrid Mesoporous Aluminosilicate Sieve Prepared with Fly Ash. *Appl. Surf. Sci.* **2013**, *273*, 706–716. [CrossRef] [PubMed]
52. Witek-Krowiak, A. Application of Beech Sawdust for Removal of Heavy Metals from Water: Biosorption and Desorption Studies. *Eur. J. Wood Wood Prod.* **2013**, *71*, 227–236. [CrossRef]
53. Mračková, E.; Adamčík, L.; Kminiak, R. Evaluation of Particle Size of Wood Dust from Tropical Wood Species by Laser Diffraction and Sieve Analysis. *Forests* **2025**, *16*, 1790. [CrossRef]
54. Zhang, Z.B.; Liu, X.Y.; Li, D.W.; Gao, T.T.; Lei, Y.Q.; Wu, B.G.; Zhao, J.W.; Wang, Y.K.; Wei, L. Effects of the Ultrasound-Assisted H_3PO_4 Impregnation of Sawdust on the Properties of Activated Carbons Produced from It. *Xinxing Tan. Cailiao/New Carbon Mater.* **2018**, *33*, 409–416. [CrossRef]
55. Nayak, A.; Bhushan, B.; Gupta, V.; Sharma, P. Chemically Activated Carbon from Lignocellulosic Wastes for Heavy Metal Wastewater Remediation: Effect of Activation Conditions. *J. Colloid Interface Sci.* **2017**, *493*, 228–240. [CrossRef] [PubMed]
56. Sciban, M.; Klasnja, M. Study of the Adsorption of Copper(II) Ions from Water onto Wood Sawdust, Pulp and Lignin. *Adsorpt. Sci. Technol.* **2004**, *22*, 195–206. [CrossRef]
57. Ferrero, F. Dye Removal by Low Cost Adsorbents: Hazelnut Shells in Comparison with Wood Sawdust. *J. Hazard. Mater.* **2007**, *142*, 144–152. [CrossRef] [PubMed]
58. Jannat, N.; Latif Al-Mufti, R.; Hussien, A.; Abdullah, B.; Cotgrave, A. Influence of Sawdust Particle Sizes on the Physico-Mechanical Properties of Unfired Clay Blocks. *Designs* **2021**, *5*, 57. [CrossRef]
59. Açıkyıldız, M.; Gürses, A.; Karaca, S. Preparation and Characterization of Activated Carbon from Plant Wastes with Chemical Activation. *Microporous Mesoporous Mater.* **2014**, *198*, 45–49. [CrossRef]
60. Miskam, A.; Zainal, Z.A.; Yusof, I.M. Characterization of Sawdust Residues for Cyclone Gasifier. *J. Appl. Sci.* **2009**, *9*, 2294–2300. [CrossRef]
61. Qiu, K.; Yang, S.; Yang, J. Characteristics of Activated Carbon Prepared from Chinese Fir Sawdust by Zinc Chloride Activation under Vacuum Condition. *J. Cent. S. Univ. Technol.* **2009**, *16*, 385–391. [CrossRef]

62. Ghani, W.A.W.A.K.; Mohd, A.; da Silva, G.; Bachmann, R.T.; Taufiq-Yap, Y.H.; Rashid, U.; Al-Muhtaseb, A.H. Biochar Production from Waste Rubber-Wood-Sawdust and Its Potential Use in C Sequestration: Chemical and Physical Characterization. *Ind. Crops Prod.* **2013**, *44*, 18–24. [CrossRef]
63. Azargohar, R.; Jacobson, K.L.; Powell, E.E.; Dalai, A.K. Evaluation of Properties of Fast Pyrolysis Products Obtained, from Canadian Waste Biomass. *J. Anal. Appl. Pyrolysis* **2013**, *104*, 330–340. [CrossRef]
64. Thomas, A.; Dabai, F.N.; Aderemi, B.O.; Sani, Y.M. Extraction of Lignin from Sawdust (*Chlorophora excelsa*). *Chem. Proc.* **2025**, *17*, 2. [CrossRef]
65. Wang, S.; Wu, H. Environmental-Benign Utilisation of Fly Ash as Low-Cost Adsorbents. *J. Hazard. Mater.* **2006**, *136*, 482–501. [CrossRef] [PubMed]
66. Adamczuk, A.; Kołodyńska, D. Equilibrium, Thermodynamic and Kinetic Studies on Removal of Chromium, Copper, Zinc and Arsenic from Aqueous Solutions onto Fly Ash Coated by Chitosan. *Chem. Eng. J.* **2015**, *274*, 200–212. [CrossRef]
67. Bhattacharya, A.K.; Naiya, T.K.; Mandalb, S.N.; Dasa, S.K. Adsorption, Kinetics and Equilibrium Studies on Removal of Cr(VI) from Aqueous Solutions Using Different Low-Cost Adsorbents. *Chem. Eng. J.* **2008**, *137*, 529–541. [CrossRef]
68. Kalavathy, M.H.; Karthikeyan, T.; Rajgopal, S.; Miranda, L.R. Kinetic and Isotherm Studies of Cu(II) Adsorption onto H_3PO_4-Activated Rubber Wood Sawdust. *J. Colloid Interface Sci.* **2005**, *292*, 354–362. [CrossRef] [PubMed]
69. Qiu, R.; Cheng, F.; Huang, H. Removal of Cd^{2+} from Aqueous Solution Using Hydrothermally Modified Circulating Fluidized Bed Fly Ash Resulting from Coal Gangue Power Plant. *J. Clean. Prod.* **2018**, *172*, 1918–1927. [CrossRef]
70. Ibrahim, A.H.; Lyu, X.; ElDeeb, A.B. Synthesized Zeolite Based on Egyptian Boiler Ash Residue and Kaolin for the Effective Removal of Heavy Metal Ions from Industrial Wastewater. *Nanomaterials* **2023**, *13*, 1091. [CrossRef] [PubMed]
71. Jiao, C.; Xiong, J.; Tao, J.; Xu, S.; Zhang, D.; Lin, H.; Chen, Y. Sodium Alginate/Graphene Oxide Aerogel with Enhanced Strength-Toughness and Its Heavy Metal Adsorption Study. *Int. J. Biol. Macromol.* **2016**, *83*, 133–141. [CrossRef] [PubMed]
72. Xiang, B.; Fan, W.; Yi, X.; Wang, Z.; Gao, F.; Li, Y.; Gu, H. Dithiocarbamate-Modified Starch Derivatives with High Heavy Metal Adsorption Performance. *Carbohydr. Polym.* **2016**, *136*, 30–37. [CrossRef] [PubMed]
73. Ali, R.M.; Hamad, H.A.; Hussein, M.M.; Malash, G.F. Potential of Using Green Adsorbent of Heavy Metal Removal from Aqueous Solutions: Adsorption Kinetics, Isotherm, Thermodynamic, Mechanism and Economic Analysis. *Ecol. Eng.* **2016**, *91*, 317–332. [CrossRef]
74. Huang, X.; Zhao, H.; Hu, X.; Liu, F.; Wang, L.; Zhao, X.; Gao, P.; Ji, P. Optimization of Preparation Technology for Modified Coal Fly Ash and Its Adsorption Properties for Cd^{2+}. *J. Hazard. Mater.* **2020**, *392*, 122461. [CrossRef] [PubMed]
75. Bao, W.; Liu, L.; Zou, H.; Gan, S.; Xu, X.; Ji, G.; Gao, G.; Zheng, K. Removal of Cu^{2+} from Aqueous Solutions Using Na-A Zeolite from Oil Shale Ash. *Chin. J. Chem. Eng.* **2013**, *21*, 974–982. [CrossRef]
76. Javadian, H.; Ghorbani, F.; Tayebi, H.a.; Asl, S.M.H. Study of the Adsorption of Cd (II) from Aqueous Solution Using Zeolite-Based Geopolymer, Synthesized from Coal Fly Ash; Kinetic, Isotherm and Thermodynamic Studies. *Arab. J. Chem.* **2015**, *8*, 837–849. [CrossRef]
77. Ajala, M.A.; Abdulkareem, A.S.; Kovo, A.S.; Tijani, J.O.; Ajala, O.E. Adsorption Studies of Zinc, Copper, And Lead Ions from Pharmaceutical Wastewater Onto Silver-Modified Clay Adsorbent. *South. J. Sci.* **2022**, *30*, 28–43. [CrossRef]
78. Shukla, S.R.; Pai, R.S. Adsorption of Cu(II), Ni(II) and Zn(II) on Dye Loaded Groundnut Shells and Sawdust. *Sep. Purif. Technol.* **2005**, *43*, 1–8. [CrossRef]
79. Mahmood-ul-Hassan, M.; Yasin, M.; Yousra, M.; Ahmad, R.; Sarwar, S. Kinetics, Isotherms, and Thermodynamic Studies of Lead, Chromium, and Cadmium Bio-Adsorption from Aqueous Solution onto Picea Smithiana Sawdust. *Environ. Sci. Pollut. Res.* **2018**, *25*, 12570–12578. [CrossRef] [PubMed]
80. Najam, R.; Andrabi, S.M.A. Adsorption Capability of Sawdust of Populus Alba for Pb(II), Zn(II) and Cd(II) Ions from Aqueous Solution. *Desalin. Water Treat.* **2016**, *57*, 29019–29035. [CrossRef]
81. Kovacova, Z.; Demcak, S.; Balintova, M.; Pla, C.; Zinicovscaia, I. Influence of Wooden Sawdust Treatments on Cu(II) and Zn(II) Removal from Water. *Materials.* **2020**, *13*, 3575. [CrossRef] [PubMed]
82. Rafatullah, M.; Sulaiman, O.; Hashim, R.; Ahmad, A. Adsorption of Copper (II), Chromium (III), Nickel (II) and Lead (II) Ions from Aqueous Solutions by Meranti Sawdust. *J. Hazard. Mater.* **2009**, *170*, 969–977. [CrossRef] [PubMed]
83. Taty-Costodes, V.C.; Fauduet, H.; Porte, C.; Delacroix, A. Removal of Cd(II) and Pb(II) Ions, from Aqueous Solutions, by Adsorption onto Sawdust of Pinus Sylvestris. *J. Hazard. Mater.* **2003**, *105*, 121–142. [CrossRef] [PubMed]
84. Sciban, M.; Klasnja, M.; Skrbic, B. Modified Softwood Sawdust as Adsorbent of Heavy Metal Ions from Water. *J. Hazard. Mater.* **2006**, *136*, 266–271. [CrossRef] [PubMed]
85. Xu, D.; Fan, D.; Shen, W. Catalyst-Free Direct Vapor-Phase Growth of Zn1−xCu x O Micro-Cross Structures and Their Optical Properties. *Nanoscale Res. Lett.* **2013**, *8*, 46. [CrossRef] [PubMed]
86. Zhu, H.; Tan, X.; Tan, L.; Chen, C.; Alharbi, N.S.; Hayat, T.; Fang, M.; Wang, X. Biochar Derived from Sawdust Embedded with Molybdenum Disulfide for Highly Selective Removal of Pb^{2+}. *ACS Appl. Nano Mater.* **2018**, *1*, 2689–2698. [CrossRef]

87. Liu, C.; Ding, S.; Feng, H. Competitive Adsorption Mechanism of Heavy Metal Ions by Lignocellulose Materials: A Review. *J. Environ. Chem. Eng.* **2026**, *14*, 123001. [CrossRef]
88. Ibrahim, N.A.; Abdellatif, F.H.H.; Hasanin, M.S.; Abdellatif, M.M. Fabrication, Characterization, and Potential Application of Modified Sawdust Sorbents for Efficient Removal of Heavy Metal Ions and Anionic Dye from Aqueous Solutions. *J. Clean. Prod.* **2022**, *332*, 130021. [CrossRef]
89. Salman, S.M.; Kamal, F.; Zahoor, M.; Wahab, M.; Shahwar, D.; Khan, H.U.; Badshah, S.L.; Shah, S.N.; Sadia, M.; Kamran, A.W. Removal of Heavy Metal Ions from Aqueous Solution Using Populus Nigra Sawdust–Based Activated Carbon. *Desalin. Water Treat.* **2021**, *221*, 239–251. [CrossRef]

Disclaimer/Publisher's Note: The statements, opinions and data contained in all publications are solely those of the individual author(s) and contributor(s) and not of MDPI and/or the editor(s). MDPI and/or the editor(s) disclaim responsibility for any injury to people or property resulting from any ideas, methods, instructions or products referred to in the content.